

Cavity QED with an ultracold ensemble on a chip: Prospects for strong magnetic coupling at finite temperatures

Kathrin Henschel,¹ Johannes Majer,² Jörg Schmiedmayer,² and Helmut Ritsch¹

¹*Institute for Theoretical Physics, Universität Innsbruck, Technikerstrasse 25, A-6020 Innsbruck, Austria*

²*Atominstitut, TU-Wien, Stadionallee 2, A-1020 Vienna, Austria*

(Received 2 July 2010; published 13 September 2010)

We study the nonlinear dynamics of an ensemble of cold trapped atoms with a hyperfine transition magnetically coupled to a resonant microwave cavity mode. Despite the minute single-atom coupling, one obtains strong coupling between collective hyperfine qubits and microwave photons, enabling coherent transfer of an excitation between the long-lived atomic qubit state and the mode. Evidence of strong coupling can be obtained from the cavity transmission spectrum even at finite thermal photon number. The system makes it possible to study further prominent collective phenomena such as superradiant decay of an inverted ensemble or the building of a narrowband stripline micromaser locked to an atomic hyperfine transition.

DOI: [10.1103/PhysRevA.82.033810](https://doi.org/10.1103/PhysRevA.82.033810)

PACS number(s): 37.30.+i, 42.50.Pq

I. INTRODUCTION

The idea of resonant coupling of an ensemble of atoms to a single cavity mode has been addressed in numerous aspects and contexts, some dating back several decades [1]. Recently, in the context of quantum information processing, such Hamiltonians attracted renewed attention because the ensemble can serve as quantum memory with long coherence times [2–5]. Despite small coupling of individual atoms, the strong collective coupling of the ensemble to a particular cavity mode allows for the coherent transfer of an excitation to the ensemble, its storage and its retrieval after some time shorter than the coherence time of the system. Hence, due to collective effects, one can utilize atomic transitions and geometries for which the strong coupling regime would not be accessible otherwise.

As a particularly striking example, one can even envisage the use of states that are very weakly coupled to the field, for example, an optically forbidden hyperfine transition, which only couple to the field via magnetic dipole interaction. What makes this idea attractive and possibly feasible with current technology is the fact that it should be possible to fabricate high- Q stripline waveguide cavities on the superconducting surface of a microchip, which confine the microwave mode to a very small effective volume and to simultaneously trap a large ensemble of cold atoms very close to the surface. The combination of high- Q stripline waveguide cavities and atom-trapping technology surely will involve new challenges, but there seem to be no fundamental problems. As already demonstrated, such a cavity can be strongly coupled to on-chip Cooper-pair box qubits [6]. By combining the two systems, one thus could establish a connection between the atomic ensemble and solid-state qubits. This setup hence bridges an enormous range of time scales starting from the submicrosecond scale of solid-state qubits, over the millisecond lifetime of microwave photons, to the atomic hyperfine coherence lifetime of seconds.

In the particular setup discussed here, the ensemble consists of a cloud of ultracold ^{87}Rb trapped in an on-chip magnetic wire trap and pumped to one of the trappable hyperfine levels, for example, $F = 1$, $m_F = -1$. The interaction between the atoms and the field is dominated by the magnetic dipole

transitions between $|F = 1, m_F\rangle$ and $|F = 2, m'_F\rangle$. These transitions are widely used for hyperfine manipulations of cold atomic ensembles by externally injected microwaves [7]. We assume in the following that the experimental setup guarantees that the cavity is resonant with only one of the possible transitions (e.g. $m_F = -1$ and $m'_F = 1$ with transition frequency $\omega_a/(2\pi) = 6.83$ GHz, corresponding to $T \approx 330$ mK), and hence allows for the atoms to be treated as two-level systems. Actually, in some cases it is more favorable to use Raman-type coupling employing an extra radio-wave field to choose a suitable microwave transition [8].

We ignore some of these technical details at this point and focus on the three main topics: After the introduction of the model in Sec. II, we first investigate conditions for strong coupling between the ensemble and the cavity and the experimental consequences when one adds the obscuring effects of thermal photons due to a finite cavity temperature. In Secs. III A and III B we discuss the methods we use, whereas in Secs. III C–III F we address several aspects of the resulting dynamics. Here the optically aligned ensemble, which has much lower effective temperature, can be expected to act as a heat sink for the cavity mode removing thermal photons. As the upper and lower hyperfine states have a virtually infinite lifetime compared with other system time scales, we can also completely invert the system, mimicking an effective negative temperature, and use it to pump energy into the system. As a prominent example, we study in Sec. IV the superradiant decay of a fully inverted ensemble again with some thermal photons initially present. Finally, we exhibit in Sec. V the possibility of building an ultranarrow linewidth single-chip stripline micromaser operating directly on an atomic clock type transition, which is in close analogy to an optical-lattice-based setup, as recently suggested in [9].

II. MODEL

A. Collective atom-field Hamiltonian

A single atom, formally represented here by a two-level system resonantly coupled to a cavity mode, can be well described by the Jaynes-Cummings Hamiltonian. For N two-level systems trapped so close to each other in the cavity that

they see the same field and thus are coupled to the mode with equal strength g , we then get the generalized Hamiltonian:

$$H = \hbar\omega_m a^\dagger a + \frac{\hbar\omega_a}{2} \sum_j \sigma_j^z + \hbar g \sum_j (\sigma_j^+ a + a^\dagger \sigma_j^-), \quad (1)$$

with a being the annihilation operator for a cavity photon, σ_j^\pm being the excitation operator for the j th two-level system, and $[\sigma_i^+, \sigma_j^-] = \sigma_i^z \delta_{ij}$. The frequency of the two-level systems and the mode are denoted by ω_a and ω_m , respectively. The coupling strength $g = \vec{B}(\vec{r}) \cdot \vec{\mu}/\hbar$ depends on the strength of the magnetic field per photon \vec{B} at the position \vec{r} of the atoms and the magnetic moment $\vec{\mu}$ of the considered transition.

What make an ensemble of atoms coupled to a cavity interesting are collective effects emerging from the common coupling of all atoms to the same mode. This can be well illustrated by introducing collective atomic operators $S^\pm = \sum_j \sigma_j^\pm$ and $S^z = \frac{1}{2} \sum_j \sigma_j^z$. The treatment in terms of collective operators provides a convenient basis for classifying the possible states of the ensemble and is therefore discussed here. As we see in Sec. II B, we have to resort to Hamiltonian (1) in our particular treatment. The introduction of S^\pm and S^z leads to the Tavis-Cummings form of this Hamiltonian:

$$H_{\text{TC}} = \hbar\omega_m a^\dagger a + \hbar\omega_a S^z + \hbar g (S^+ a + a^\dagger S^-), \quad (2)$$

where single photons are coupled to distributed (delocalized) excitations in the ensemble [1]. Let us shortly review some of its most known properties here. Mathematically, the collective operators follow the standard commutation relations for angular momentum operators $\mathbf{S} = (S^x, S^y, S^z)$, with $S^\pm = (S^x \pm iS^y)$. The corresponding eigenstates of S^2 and S^z are the so-called Dicke states $|J, M\rangle$, with $S^2|J, M\rangle = J(J+1)|J, M\rangle$ and $S^z|J, M\rangle = M|J, M\rangle$, where $J = 0, 1, \dots, N/2$ and $M = -J, \dots, J$. Formally, a fully inverted ensemble corresponds to the maximum angular momentum of $J = N/2$ [10,11] and projection $M = N/2$. Repeated application of the collective downward ladder operator S^- on the initial state $|J, J\rangle \hat{=} |e, e, \dots, e\rangle$ gives the lowest state $|J, -J\rangle \hat{=} |g, g, \dots, g\rangle$.

The states in between are generated according to

$$S^\pm |J, M\rangle = \sqrt{(J \pm M + 1)(J \mp M)} |J, M \pm 1\rangle. \quad (3)$$

The interaction can then be conveniently rewritten in terms of normalized collective operators $\tilde{S}^\pm = \frac{1}{\sqrt{N}} \sum_i \sigma_i^\pm$ to obtain

$$\tilde{H} = \hbar\omega_m a^\dagger a + \hbar\omega_a \tilde{S}^+ \tilde{S}^- + \hbar g_{\text{eff}} (\tilde{S}^+ a + a^\dagger \tilde{S}^-), \quad (4)$$

with $g_{\text{eff}} = g\sqrt{N}$. Note that in the case where the atoms in the ensemble couple to the cavity with different coupling constants g_i , we generalize to $\tilde{S}^\pm = \frac{1}{g_{\text{eff}}} \sum_i g_i \sigma_i^\pm$, with $g_{\text{eff}} = \sqrt{\sum_i g_i^2}$. This reduces to $g_{\text{eff}} = g\sqrt{N}$ if all g_i are equal. To simplify matters, we remain with the case of equal coupling strength.

Allowing only one excitation in the system, we see that the ground state $|0\rangle_a \hat{=} |J, -J\rangle \hat{=} |g, g, \dots, g\rangle$ is only coupled to the symmetric atomic excitation state $\tilde{S}^+ |0\rangle_a = |1\rangle_a = |J, -J+1\rangle \hat{=} \frac{1}{\sqrt{N}} (|e, g, g, \dots, g\rangle + |g, e, g, \dots, g\rangle + \dots + |g, \dots, g, e\rangle)$, while other atomic states with only one excitation play no role. Hence, in this form we end up again with a two-level atomic system, where the

dependence of the atom-cavity coupling on the number of atoms is explicitly visible. Even for transitions with a very small coupling constant g , strong coupling can be achieved for sufficiently large N .

Note that in Eq. (4) we use $\tilde{S}^z \approx -\frac{1}{2} + \frac{\tilde{S}^+ \tilde{S}^-}{N}$, where $\tilde{S}^z = \frac{1}{2N} \sum_i \sigma_i^z$. This approximation is exactly valid only either for a single atom or the special case where we consider only one excitation in the system. The constant $-\frac{1}{2}$ is neglected in the Hamiltonian. In general, we find for a state with $J = \frac{N}{2}$ and $M = -J + s$

$$\langle J, -J + s | \tilde{S}^z | J, -J + s \rangle = -\frac{1}{2} + \frac{s}{2J} \quad (5)$$

and

$$\langle J, -J + s | \tilde{S}^+ \tilde{S}^- | J, -J + s \rangle = s - \frac{s(s-1)}{2J}. \quad (6)$$

For $s \ll N$ we neglect the second term on the right-hand side of Eq. (6) and find the approximation for \tilde{S}^z , which becomes exact for $s = 1$.

For large ensembles with few excitations this approximation is closely related to the bosonization procedure. For $M \approx -J$ with $J = N/2$ and from

$$[\tilde{S}^+, \tilde{S}^-] = \frac{1}{N} [S^+, S^-] = \frac{2S^z}{N} = \left[-1 + O\left(\frac{1}{N}\right) \right] \mathbf{1}, \quad (7)$$

we find that for few excitations it is possible to identify \tilde{S}^+ and \tilde{S}^- with bosonic creation and annihilation operators. Hence, we end up with a system of coupled oscillators, for which a great deal of solution techniques exist.

Let us now come back to the atom-field interaction [Eq. (4)]. It is well known that the eigenstates are coherent superpositions of the two previously introduced basis states, where the excitation is located either in the mode or in the ensemble. Let $|0\rangle_m$ and $|1\rangle_m = a^\dagger |0\rangle_m$ be the possible states of the mode and $|0\rangle_a$ and $|1\rangle_a$ be the ensemble states. With $\omega_a = \omega_m$, the two eigenstates then read

$$|+\rangle = \frac{1}{\sqrt{2}} (|1\rangle_a |0\rangle_m + |0\rangle_a |1\rangle_m), \quad (8)$$

$$|-\rangle = \frac{1}{\sqrt{2}} (|1\rangle_a |0\rangle_m - |0\rangle_a |1\rangle_m), \quad (9)$$

and as expected are separated by the energy difference $2g_{\text{eff}}$. Of course, the system possesses more states containing essentially one excitation quantum, but those are not directly coupled to the ground state if we consider only collective operators. The collective operators couple states within one J manifold, like the previously discussed manifold with maximum angular momentum $J = N/2$ and $M = -J \dots J$. Taking into account the manifolds of states with $J < N/2$, one can see that in general there is a large number of states describing an ensemble with n excitations. In the forthcoming calculations including spontaneous emissions, such states with $J < N/2$ can be populated as well [12]. In addition, we also do not restrict the dynamics to a single excitation.

B. Master equation including decoherence and thermal noise

In any realistic implementation of the preceding model, coupling of the thermal environment to the field mode and the

atoms is unavoidable. This generates several sources of noise and decoherence we have to address to be able to reliably describe the dynamics. Despite its high Q value, the microwave resonator still has a non-negligible finite linewidth $\kappa = 1/\tau$. In other words, a stored photon is likely to be lost from the cavity after the time τ . Similarly, atomic excitations are assumed to decay with a rate that is, fortunately, in our case negligibly small in practice [13]. However, we have to consider trap loss of atoms leaving the cavity mode, which generates an effectively faster decay of the atomic excitation, denoted by the rate γ_a . This can be to some extent controlled by a suitable choice of the trapping states and trap geometry. An additional and in general quite serious source of noise are thermal photons that leak into the cavity. For an unperturbed cavity mode they lead to an average occupation number of

$$\bar{n}(\omega_m, T) = \frac{e^{-\frac{\hbar\omega_m}{k_B T}}}{1 - e^{-\frac{\hbar\omega_m}{k_B T}}}, \quad (10)$$

where T denotes the temperature of the environment. In principle, such thermal photons are also present on the atomic transition and lead to a thermalization of the optically pumped atomic ensemble. Fortunately, the weak dipole moment of the atom renders this thermalization rate so slow that it can be ignored at the experimentally relevant time scales. In principle, even this rate could be collectively enhanced, but it largely addresses collective states only very weakly coupled to the cavity mode.

Putting all these noise sources together, we can use standard quantum optical methods to derive a corresponding master equation for the reduced atom-cavity density matrix [14]:

$$\frac{d}{dt}\rho = \frac{1}{i\hbar}[H, \rho] + \mathcal{L}[\rho], \quad (11)$$

with the Liouvillian

$$\begin{aligned} \mathcal{L}[\rho] &= \mathcal{L}_{\text{cavity}}[\rho] + \mathcal{L}_{\text{spont}}[\rho] \\ &= \kappa(\bar{n} + 1)(2a\rho a^\dagger - a^\dagger a\rho - \rho a^\dagger a) \\ &\quad + \kappa\bar{n}(2a^\dagger \rho a - a a^\dagger \rho - \rho a a^\dagger) \\ &\quad - \frac{\gamma_a}{2} \sum_{j=1}^N (\sigma_j^+ \sigma_j^- \rho + \rho \sigma_j^+ \sigma_j^- - 2\sigma_j^- \rho \sigma_j^+). \end{aligned} \quad (12)$$

We assumed here that direct thermal excitations of the atoms can be neglected due to the weak coupling of the hyperfine transition to the environment. The only significant influx of thermal energy thus occurs via the cavity input-output couplers (mirrors). Note that the part of the Liouvillian describing spontaneous emission reflects the assumption that the atoms are coupled to N statistically independent reservoirs. The main reason for this treatment is that the decay rate γ_a summarizes the very small decay rate of atomic excitations and the loss rate of atoms from the trap. Since the loss of individual atoms from the trap is a noncollective process, the independent reservoirs assumption is advisable. This part of the Liouvillian cannot be written in terms of collective operators, and therefore it will not conserve J [15]. Therefore, states with $J < N/2$, including dark states, become accessible.

III. SIGNATURES OF STRONG COUPLING

A decisive first step toward applications of such system is the precise characterization and determination of their limits. In particular, the experimental confirmation of sufficiently strong atom-field coupling compared to the inherent decoherence processes is of vital importance. This has to be seen in connection with extra limitations induced by thermal photons in the mode, which in contrast to optical setups play an important role in the microwave domain. We thus need reliable methods to determine the atom number, their effective coupling strength, and noise properties. In particular, we want to find the minimum temperature requirements that would make it possible to observe strong coupling.

A. Numerical solution for small particle number

To get some first qualitative understanding of finite T effects, we study the coupled atom-field dynamics in the regime of strong coupling under the influence of thermal photons based on the direct numerical solution of the master equation. Of course, here we have to resort to the limit of only a few atoms with increased coupling per particle. Nevertheless, at least the qualitative influence of thermal photons will become visible. For the practical implementation, we rely on the quantum optics toolbox for MATLAB to explicitly calculate the dynamics of the density matrix [16], which allows straightforward implementation of the Hamiltonian in Eq. (2) formulated in terms of the collective operators.

The cavity is pumped by a coherent microwave field with frequency ω_l and strength η , which in the frame rotating with ω_l is represented in the Hamiltonian by the additional term $H_p = i\hbar(\eta a^\dagger - \eta^* a)$. From the stationary solution, we then determine the steady-state photon number in the cavity for different frequencies of the pump field to determine the central system resonances, where the pump frequency matches the eigenfrequencies $\omega_m \pm g_{\text{eff}}$ of the coupled ensemble-cavity system. At zero temperature and weak pumping, we get the well-known vacuum Rabi splitting showing two distinct resonances separated by $2g_{\text{eff}}$. With increasing temperature and number of thermal photons, these two peaks will get increasingly broadened and reside on a broad background. Figure 1(a) illustrates the effect.

To compare the dynamics obtained from the restricted Tavis-Cummings Hamiltonian H_{TC} in Eq. (2) with the dynamics of Hamiltonian H in Eq. (1), we compare the results for both cases in Fig. 1(b). Even for the rather small atom numbers chosen here, the difference and thus the influence of the nonsymmetric states is hardly visible in this observable.

The peaks in the photon number in principle stay visible also for higher temperatures, but they start to broaden and finally vanish. Regardless, the detection on the thermal background gets technically more challenging. The intracavity steady-state amplitude of the field shows a similar behavior and a determination of the splitting becomes increasingly impossible, despite the fact that phase-sensitive detection (homodyne) can help. An example is shown in Fig. 2. This effect is expected to be less important if the ensemble contains a large number of atoms. However, this regime is not accessible for direct

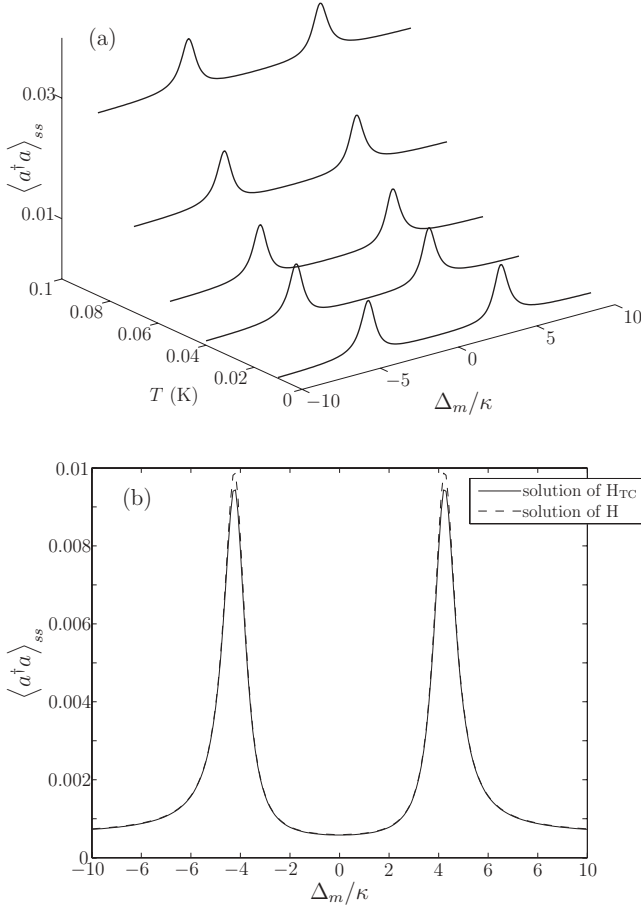


FIG. 1. (a) Steady-state number of photons $\langle a^\dagger a \rangle_{ss}$ in the pumped cavity for different detunings $\Delta_m = \omega_m - \omega_l$ and different temperatures, obtained from Hamiltonian H_{TC} . The parameters chosen were $\kappa = 1$, $N = 2$, $g = 3$, $\gamma_a = 0.05$, $\eta = 0.1$. With increasing temperature the two peaks indicating strong coupling are superimposed by thermal photons. To compare the dynamics of H_{TC} and H , we plot both results for $T = 0.04$ K ($\bar{n} = 3 \times 10^{-4}$) in (b).

numerical simulations and we have to develop alternative semianalytic approaches.

B. Truncated cumulant expansion of collective observables

To overcome the system size restrictions of a direct numerical solution, we now turn to an alternative approach that does not rely on the simulation of the dynamics of the whole density matrix. Instead, we derive a system of coupled differential equations for the expectation values of the relevant system variables. The inversion of atom i then obeys

$$\begin{aligned} \frac{d}{dt} \langle \sigma_i^z \rangle &= \text{Tr} \left\{ \sigma_i^z \frac{d}{dt} \rho \right\} \\ &= -i2g(\langle \sigma_i^+ a \rangle - \langle \sigma_i^- a^\dagger \rangle) - \gamma_a(\langle \sigma_i^z \rangle + 1), \end{aligned} \quad (13)$$

which couples to $\langle \sigma_i^+ a \rangle$ and $\langle \sigma_i^- a^\dagger \rangle = \langle \sigma_i^+ a \rangle^*$. We assume that all atoms are equal, which allows us to replace $\langle \sigma_i^z \rangle$ with $\langle \sigma_1^z \rangle$. Expectation values for pairs of different atoms like $\langle \sigma_i^+ \sigma_j^- \rangle$ can be replaced with $\langle \sigma_1^+ \sigma_2^- \rangle$.

While these equations are exact in principle, the procedure ultimately leads to an infinite set of coupled equations. We thus have to start approximations and truncate this set at a chosen point, neglecting higher-order cumulants [9,17]. The truncation has to be carefully chosen and tested in general. Here we stop at third order, which in similar situations has proven to be well suited to describe the essential correlations [9].

The expansion for an expectation value of the form $\langle ab \rangle$ is the well-known relation $\langle ab \rangle = \langle ab \rangle_c + \langle a \rangle \langle b \rangle$, with $\langle ab \rangle_c$ being the covariance between a and b . Along this line, one expands third-order terms in the form

$$\begin{aligned} \langle abc \rangle &= \underbrace{\langle abc \rangle_c}_{\text{neglected}} + \langle ab \rangle_c \langle c \rangle + \langle ac \rangle_c \langle b \rangle \\ &+ \langle bc \rangle_c \langle a \rangle + \langle a \rangle \langle b \rangle \langle c \rangle. \end{aligned} \quad (14)$$

We make one exception in this expansion when it comes to the quantity $\langle a^\dagger a \sigma_1^z \rangle$; the reason for this is discussed in Appendix B.

The number of equations depends on the order of the cumulants we wish to keep track of. Furthermore, the problem is greatly simplified if there is no coherent input field driving our cavity. In this case, no defined phase exists in our system, so we can assume that $\langle a \rangle = \langle a^\dagger \rangle = \langle \sigma_1^\pm \rangle = 0$. Note that while for a single system trajectory a coherent field can build up as in a laser, for an average over many realizations the preceding assumption holds. For a covariance like $\langle \sigma_1^+ a \rangle_c = \langle \sigma_1^+ a \rangle - \langle \sigma_1^+ \rangle \langle a \rangle$, we therefore find $\langle \sigma_1^+ a \rangle = \langle \sigma_1^+ a \rangle_c$. The four remaining equations are

$$\frac{d}{dt} \langle \sigma_1^z \rangle = -i2g(\langle \sigma_1^+ a \rangle - \langle \sigma_1^- a^\dagger \rangle) - \gamma_a(\langle \sigma_1^z \rangle + 1), \quad (15)$$

$$\begin{aligned} \frac{d}{dt} \langle a \sigma_1^+ \rangle &= -\left(\kappa + \frac{\gamma_a}{2} + i(\omega_m - \omega_a) \right) \langle a \sigma_1^+ \rangle \\ &- ig \left(\frac{\langle \sigma_1^z \rangle + 1}{2} + \langle a^\dagger a \rangle \langle \sigma_1^z \rangle + (N-1) \langle \sigma_1^+ \sigma_2^- \rangle \right), \end{aligned} \quad (16)$$

$$\frac{d}{dt} \langle a^\dagger a \rangle = -igN(\langle a^\dagger \sigma_1^- \rangle - \langle a \sigma_1^+ \rangle) - 2\kappa \langle a^\dagger a \rangle + 2\kappa \bar{n}, \quad (17)$$

$$\frac{d}{dt} \langle \sigma_1^+ \sigma_2^- \rangle = -\gamma_a \langle \sigma_1^+ \sigma_2^- \rangle - ig \langle \sigma_1^z \rangle (\langle \sigma_1^- a^\dagger \rangle - \langle \sigma_1^+ a \rangle). \quad (18)$$

To inject energy into our system without losing the property of having no defined phase, we can introduce an incoherent pump of the atoms. In essence, this gives an additional term in the Liouvillian very much resembling spontaneous emission in opposite direction. Formally, it reads $-\frac{w}{2} \sum_{j=1}^N (\sigma_j^- \sigma_j^+ \rho + \rho \sigma_j^- \sigma_j^+ - 2\sigma_j^+ \rho \sigma_j^-)$, where w denotes the rate of the pump. The modifications of Eqs. (15)–(18) narrow down to the replacement of γ_a with $\gamma_a + w$ and of $-\gamma_a(\langle \sigma_1^z \rangle + 1)$ with $-(\gamma_a + w)(\langle \sigma_1^z \rangle + \frac{w - \gamma_a}{w + \gamma_a})$ in Eq. (15).

Introducing a coherent pump leads to a larger set of 13 coupled equations for the quantities $\langle a \rangle$, $\langle \sigma_1^z \rangle$, $\langle \sigma_1^+ \rangle$, $\langle a \sigma_1^+ \rangle_c$, $\langle a \sigma_1^z \rangle_c$, $\langle \sigma_1^+ \sigma_2^- \rangle_c$, $\langle a^\dagger a \rangle$, $\langle a \sigma_1^- \rangle_c$, $\langle a^\dagger a^\dagger \rangle_c$, $\langle \sigma_1^- \sigma_2^- \rangle_c$, $\langle \sigma_1^z \sigma_2^z \rangle_c$, $\langle \sigma_1^z \sigma_2^z \rangle_c$, and $\langle a^\dagger a \sigma_1^z \rangle$; for details, see Appendix A. In this case we transform into a rotating frame with respect to the frequency of the pump ω_l . This results in $\Delta_m = \omega_m - \omega_l$ for the detuning

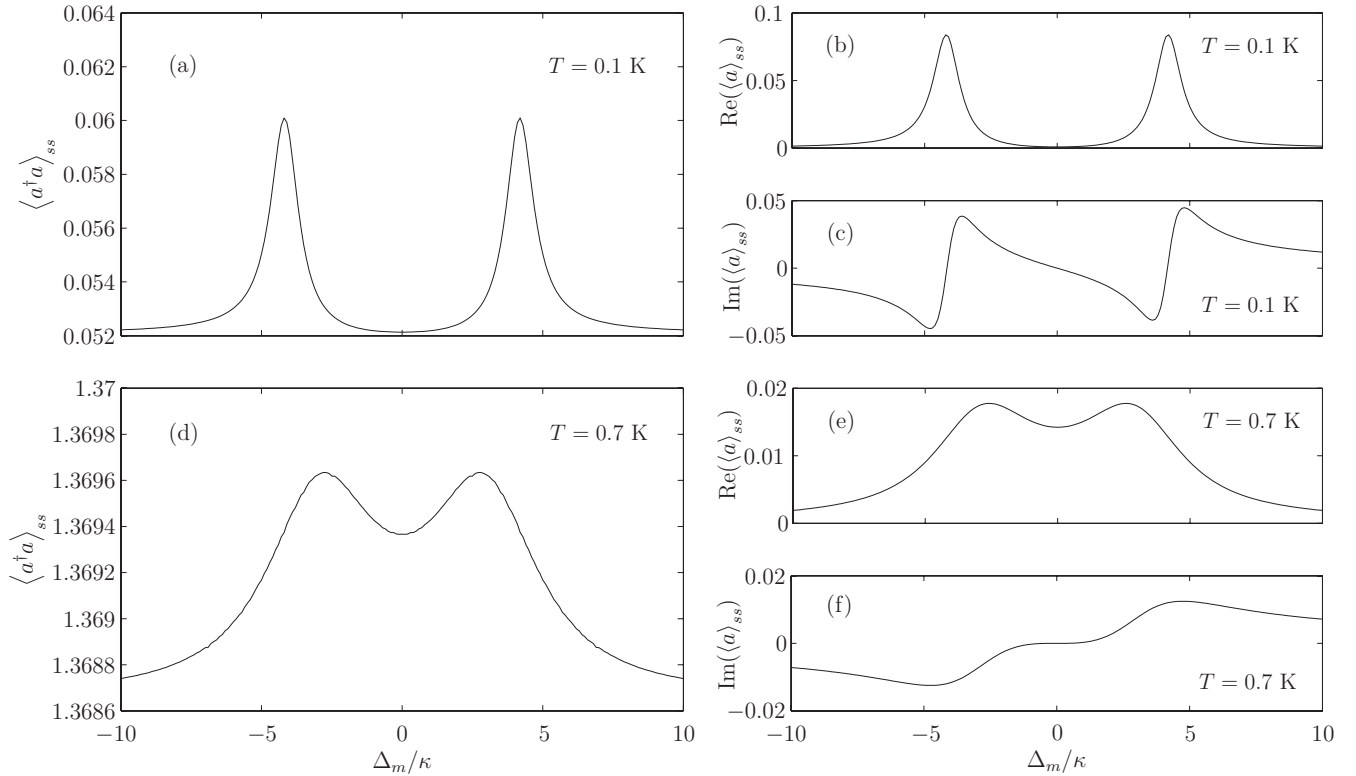


FIG. 2. Effects of higher temperatures: For $T = 0.1 \text{ K}$, (a) shows the steady-state number of photons, whereas (b) and (c) show the real and imaginary part of the steady state field in the cavity. The peaks in the photon number start to broaden and finally vanish. The amplitude of the field shows similar behavior. Panels (d), (e), and (f) show the same quantities for $T = 0.7 \text{ K}$. The remaining parameters were chosen as in Fig. 1.

of the cavity and $\Delta_a = \omega_a - \omega_l$ for the detuning of the atoms with respect to the pump frequency.

In general, the set of equations is too complex for a direct analytical solution and has to be integrated numerically. In this way we obtain the steady-state expectation values of relevant observables as the occupation number of the cavity $\langle a^\dagger a \rangle$ or the inversion of the ensemble $\langle \sigma_1^z \rangle$.

To compare the results of the obtained equations with the results in Sec. III A, we plot the steady-state number of photons and the field in the cavity for different frequencies of the pump laser in Fig. 3. We clearly see that effective strong coupling appears for a sufficiently large number of weakly coupled atoms and can stay visible also at higher temperatures. Further discussion is given in Sec. III E. In Fig. 4 we schematically depict the setup including the described loss and pump processes.

C. Cavity output spectrum at finite temperature

Naturally, the total field intensity in the cavity is only part of the story and significant physical information can be obtained from a spectral analysis of the transmitted field. Using the quantum regression theorem, the spectrum of the light transmitted through one of the mirrors can be expressed in terms of the Fourier transform of the corresponding autocorrelation function of the field amplitude.

At finite T this is not the full story, and to obtain the actual spectrum of the light impinging on the detector, one has to include the thermal photons in the output mode reflected

from the cavity. Hence, the normalized first-order correlation function of the field outside the cavity will have additional contributions from the correlation function of the thermal field, as well as of the correlation between the thermal field and the cavity field [18]. The latter is causing interference effects between cavity field and the thermal field. The correlations between reservoir operators and cavity operators can be expressed in terms of averages involving cavity operators alone [15,18]. For a cavity radiating into a thermal reservoir, we find for the normalized first-order correlation function

$$g(\tau) = \frac{1}{\mathcal{N}} \left\{ \frac{1}{2\pi g(\omega)} \langle r_f^\dagger(0) r_f(\tau) \rangle + 2\kappa \left[\lim_{t \rightarrow \infty} \langle a^\dagger(t) a(t+\tau) \rangle \right] + 2\kappa \bar{n}(\omega_m, T) \left[\lim_{t \rightarrow \infty} \langle [a^\dagger(t), a(t+\tau)] \rangle \right] \right\}, \quad (19)$$

with

$$\mathcal{N} = \frac{1}{2\pi g(\omega)} \langle r_f^\dagger r_f \rangle + 2\kappa [\langle a^\dagger a \rangle_{ss} - \bar{n}(\omega_m, T)]. \quad (20)$$

Here, r_f denotes the annihilation operator of a reservoir photon and $g(\omega)$ denotes the density of states in the reservoir. Equations for the correlation functions in Eq. (19) can be obtained via the quantum regression theorem. The resulting system of coupled equations is Laplace transformed to give the contributions to the spectrum that arise from the reservoir, the cavity and cavity-reservoir interference. The initial conditions necessary for the Laplace transform are the steady-state values obtained either numerically for the coherently pumped cavity or analytically (see Sec. V).

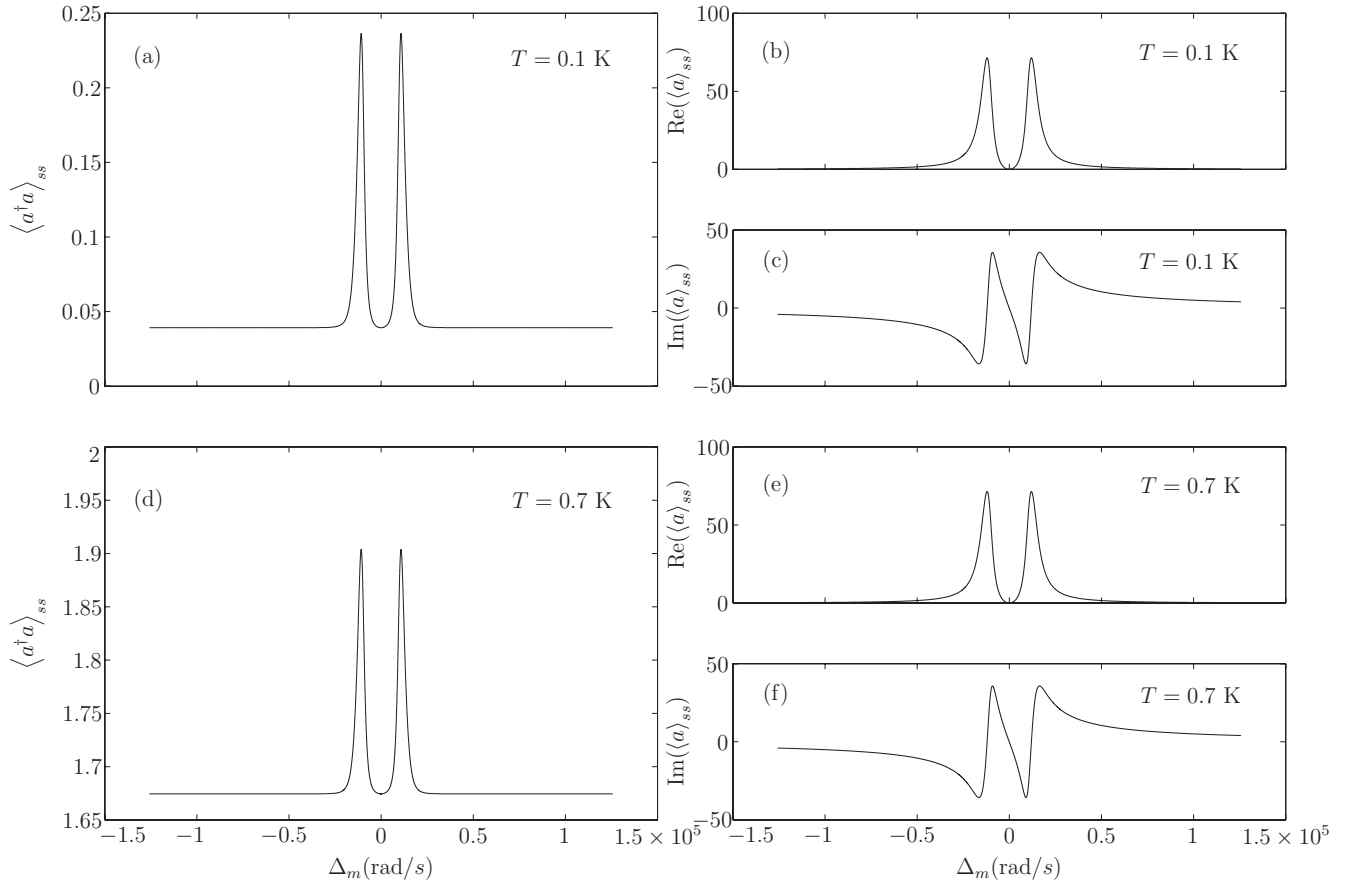


FIG. 3. The steady-state field and photon number in the cavity for different frequencies of the pump. The size of the ensemble was chosen to be $N = 10^5$ and we set $\kappa = 7 \times 10^3$, $\eta = 5 \times 10^5$, $\gamma_a = 0.3$, and $g = 40$. Panel (a) shows the steady-state number of photons, whereas (b) and (c) show the real and imaginary parts of the steady-state field in the cavity for $T = 0.1$ K, which corresponds to $\bar{n} = 0.04$. The remaining figures show the same quantities for $T = 0.7$ K, corresponding to $\bar{n} = 1.67$. The results show that for a sufficiently large number of atoms strong coupling remains observable despite of the presence of thermal photons.

We show the spectrum of the cavity without any pump, coherent or incoherent, but with $T = 0.1$ K in Fig. 5. The spectrum shows absorption dips at the frequencies of the coupled ensemble-cavity system. Some thermal photons that leak into the cavity are absorbed and lost into modes other than the cavity mode. In this form the thermal field is a broadband probe of resonant system absorption.

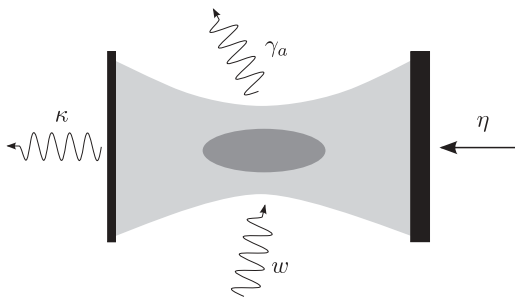


FIG. 4. To simplify matters, we depict the cavity as a Fabry-Perot cavity which can be pumped through a mirror with high reflectivity. The observation of the dynamics is carried out using the second mirror, which has a lower reflectivity. Additionally, we can pump the ensemble incoherently from the side.

D. Cooling the field mode with the atomic ensemble

The spectra depicted in Fig. 5 show a weak loss of thermal photons from the coupled ensemble-cavity system. Cavity photons are absorbed and sometimes scattered into a mode other than the cavity mode. As the ensemble can be nearly perfectly optically pumped into a particular state, its effective temperature is close to zero and hence well below the mode temperature. A relative purity of the ensemble of 10^{-5} corresponds to $T \sim 28$ mK, where we used $\hbar\omega_a/k_bT = \ln(10^{-5})$ with $\omega_a/2\pi = 6.83$ GHz. This leads to the question as to what extent the thermal occupation of the mode can be reduced by thermal contact between the two systems via such energy transfer and loss. In Fig. 6(a) we show the dynamics of the photon number in the mode at different temperatures after putting the systems into contact. In Fig. 6(b) we consider different loss or decay rates γ_a of the excited atoms. In practice one could think of coupling to a magnetically untrapped atomic state or adding some repumping mechanism to increase this intrinsically very low rate. The dynamics is found numerically by integrating Eqs. (15)–(18). To see the effect for increasing temperature in Fig. 6(a), we initialize the ensemble with all atoms in the ground state, whereas the mode contains $\bar{n}(\omega_m, T)$ photons. The decay rate of the atoms is chosen to be

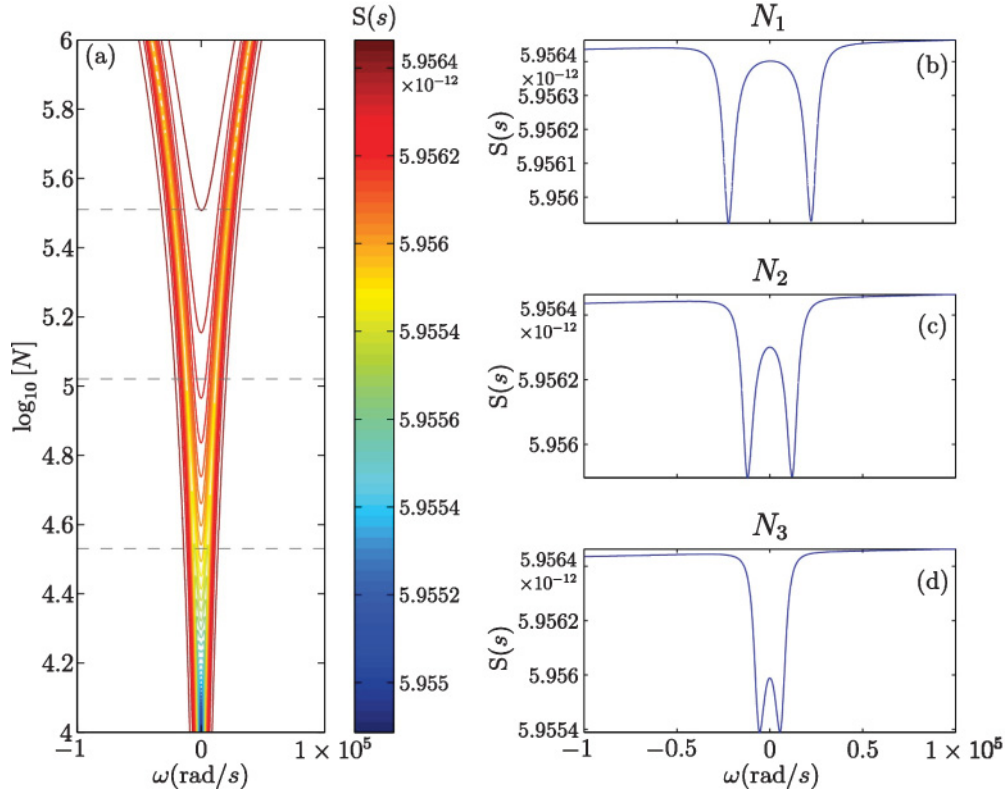


FIG. 5. (Color online) Overview of the transmitted spectrum S for different sizes of the ensemble (a). The temperature of the cavity is set to $T = 0.1$ K ($\bar{n} = 0.04$). The remaining parameters were chosen to be $\kappa = 7 \times 10^3$, $\gamma_a = 0.3$, $g = 40$, $\omega_a = \omega_m = 2\pi \times 6.83$ GHz. The dips in the spectrum indicate that thermal photons are absorbed by the ensemble and re-emitted into modes other than the cavity mode. The increasing distance between the absorption dips reflects the increasing number of atoms. In panels (b)–(d) we depict the spectra at $N_1 = 3.2 \times 10^6$, $N_2 = 1 \times 10^6$, and $N_3 = 3.4 \times 10^5$, indicated in (a) by the dashed horizontal lines.

$\gamma_a = 5 \times 10^4$. With increasing temperature the initial number of photons also increases. Due to coherent transfer and decay via the atoms, a constant fraction of the photons is removed from the cavity mode. In Fig. 6(b) we show the same effect except that we now keep the temperature fixed to $T = 4$ K and vary the decay of the atoms $\gamma_a = 1 \times 10^3 \dots 2 \times 10^5$. The steady state of the photon number strongly depends on γ_a . The red curve (with diamond markers) is the expected number of photons remaining in the cavity

$$\langle a^\dagger a \rangle_{ss} = \bar{n}(\omega_m, T) - \frac{1}{2\kappa} N \gamma_a \left(\frac{1 + \langle \sigma_1^z \rangle_{ss}}{2} \right), \quad (21)$$

which coincides with the numerical results. The inversion $\langle \sigma_1^z \rangle_{ss}$ can be calculated analytically from Eqs. (15)–(18). The loss of thermal photons is proportional to the loss rate γ_a and the number of atoms in the excited state $N \left(\frac{1 + \langle \sigma_1^z \rangle_{ss}}{2} \right)$. The latter becomes very small if γ_a becomes large. Hence there is an optimal loss rate for each set of parameters.

The removal of thermal photons becomes more effective if the number of atoms is increased. Meanwhile, the inversion of the ensemble also drops since the fraction of excited atoms is decreased. Overall, the effect is clearly visible (see Fig. 7), but it seems that for the actual parameters here its practical value remains limited. However, with a larger atom number and more tailored decay rates the method could be employed to reset a particular mode shortly before starting any quantum gate operation. Note that this treatment of the cooling process

is limited to short time scales since the permanent loss of excitations via γ_a involves the loss of atoms from the ensemble. The number of lost atoms after the time t , approximated by the number of thermal photons that entered the cavity $t\kappa\bar{n}$, has to be much smaller than the ensemble size N , which restricts the time t .

In the situation where the mode is at $T \approx 0$ K and the atoms are subject to incoherent pumping we find increased transmission for the resonance frequencies (see Fig. 8). We again recover the \sqrt{N} dependence of the splitting of the peaks.

E. Coherently driven cavity mode

An experimentally readily accessible quantity is the cavity field amplitude, which can be deduced by phase-sensitive (homodyne) detection of the output. This quantity is much less obscured by random thermal field fluctuations than the spectral intensity in total. As a phase reference, we therefore now introduce a coherent phase stable pump of the cavity, which is again represented in the Hamiltonian by the additional term $H_p = i\hbar(\eta a^\dagger - \eta^* a)$.

As mentioned previously, a coherent pump strongly increases the number of nonvanishing cumulants and at our level of truncation leads to a set of 13 coupled equations, which can be found in Appendix A. Based on this set, we can calculate the stationary real- and imaginary part of the field in the cavity after transient dynamics. The amplitude of the field inside the cavity becomes maximal if the frequency ω_l of the driving

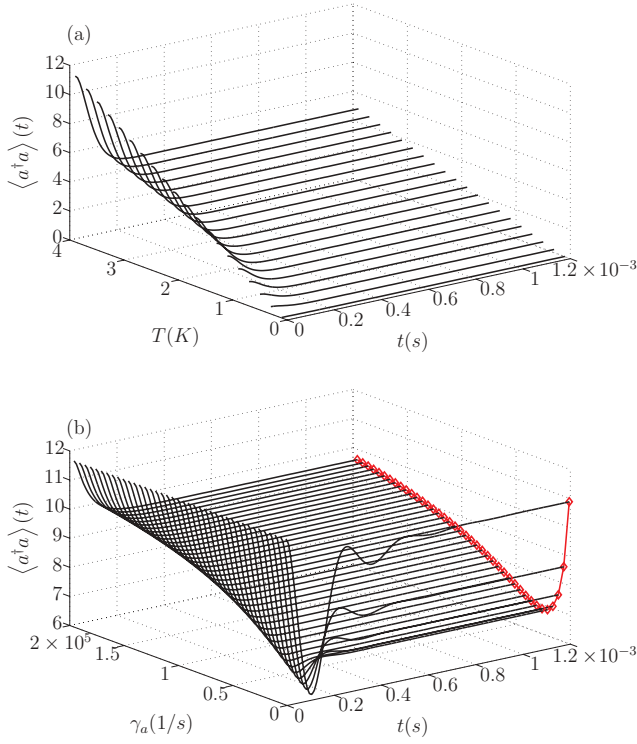


FIG. 6. (Color online) Loss of photons from the cavity mode. (a) Dynamics of the occupation of the mode for different temperatures and $\gamma_a = 5 \times 10^4$. A constant fraction of the photons is removed from the cavity mode. (b) For fixed $T = 4$ K ($\bar{n} = 11.7$), the loss rate of the atoms is varied between $\gamma_a = 1 \times 10^3$ and $\gamma_a = 2 \times 10^5$. The steady-state number of photons shows that there is an optimal loss rate. The red curve (with diamond markers) corresponds to the expected number of photons according to Eq. (21). The remaining parameters were chosen to be $\kappa = 7 \times 10^3$, $g = 40$, $\omega_a = \omega_m = 2\pi \times 6.83$ GHz, $N = 10^5$.

laser hits one of the resonances of the coupled system. As we give a phase reference now the effect of a higher temperature on the field in the cavity is barely visible, in particular if we chose a large ensemble of $N = 10^5$ atoms (see Fig. 9).

Note that although not giving the vacuum Rabi splitting, the average atom-field coupling can be still deduced from these resonances as g enters in their frequency. If we go back to a rather small ensemble of $N = 10^2$ atoms, the influence of the temperature becomes visible. To ensure that we still can observe well split levels, which are not covered by the linewidth of the cavity, we increase the coupling constant g in our simulation. The results in Fig. 10 show that thermal effects become visible in the field only if the number of thermal photons is not negligible compared to N .

F. Spectrum of the coherently driven cavity

The spectral intensity distribution of the coherently pumped cavity is calculated in a way similar to that described in Sec. III C. In contrast to the incoherent pump process that excites atoms in a noncollective way, as can be seen from the Liouvillian, the interaction with the coherently pumped mode is a collective interaction. To demonstrate this behavior, we calculate the spectral distribution of the mode intensity,

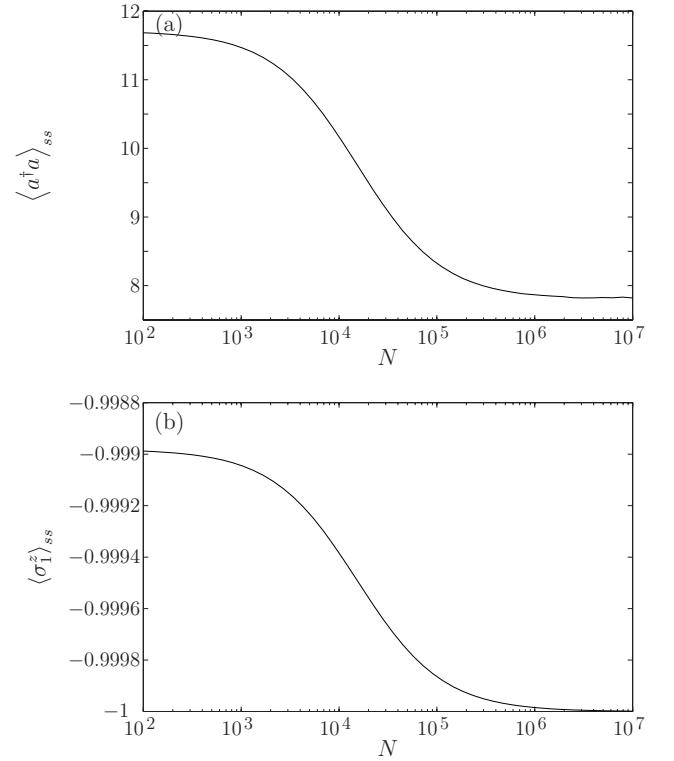


FIG. 7. Steady state of the photon number (a) and the inversion (b) for a loss rate $\gamma_a = \kappa = 7 \times 10^3$. Increasing the number of atoms N leads to a more effective removal of thermal photons. The remaining parameters are chosen to be $g = 40$, $\omega_a = \omega_m = 2\pi \times 6.83$ GHz, $T = 4$ K ($\bar{n} = 11.7$).

without caring about the reservoir it radiates into, and the spectrum of the fluorescence of the atoms.

The cavity mode and the atomic transition are assumed to be on resonance with $\omega_a = \omega_m = 2\pi \times 6.83$ GHz, which is also the frequency of the pump laser. To calculate the incoherent part of the spectra we need the Fourier transform of the two-time correlation functions

$$\begin{aligned} & \lim_{t \rightarrow \infty} \langle a^\dagger(t) a(t + \tau) \rangle_c \\ &= \lim_{t \rightarrow \infty} [\langle a^\dagger(t) a(t + \tau) \rangle - \langle a^\dagger(t) \rangle \langle a(t + \tau) \rangle] \end{aligned} \quad (22)$$

and

$$\begin{aligned} & \lim_{t \rightarrow \infty} \langle \sigma_i^+(t) \sigma_j^-(t + \tau) \rangle_c \\ &= \lim_{t \rightarrow \infty} [\langle \sigma_i^+(t) \sigma_j^-(t + \tau) \rangle - \langle \sigma_i^+(t) \rangle \langle \sigma_j^-(t + \tau) \rangle]. \end{aligned} \quad (23)$$

The quantum regression theorem and Eqs. (A1) to (A5) give

$$\begin{aligned} & \frac{d}{d\tau} \langle a^\dagger(0) a(\tau) \rangle_c \\ &= -(\kappa + i\Delta_m) \langle a^\dagger(0) a(\tau) \rangle_c - igN \langle a^\dagger(0) \sigma_i^-(\tau) \rangle_c \end{aligned} \quad (24)$$

and

$$\begin{aligned} & \frac{d}{d\tau} \langle \sigma_i^+(0) \sigma_j^-(\tau) \rangle_c = -\left(\frac{\gamma_a}{2} + i\Delta_a\right) \langle \sigma_i^+(0) \sigma_j^-(\tau) \rangle_c \\ & \quad + ig [\langle a(\tau) \rangle \langle \sigma_i^+(0) \sigma_j^z(\tau) \rangle_c \\ & \quad + \langle \sigma_i^z(\tau) \rangle \langle \sigma_i^+(0) a(\tau) \rangle_c], \end{aligned} \quad (25)$$

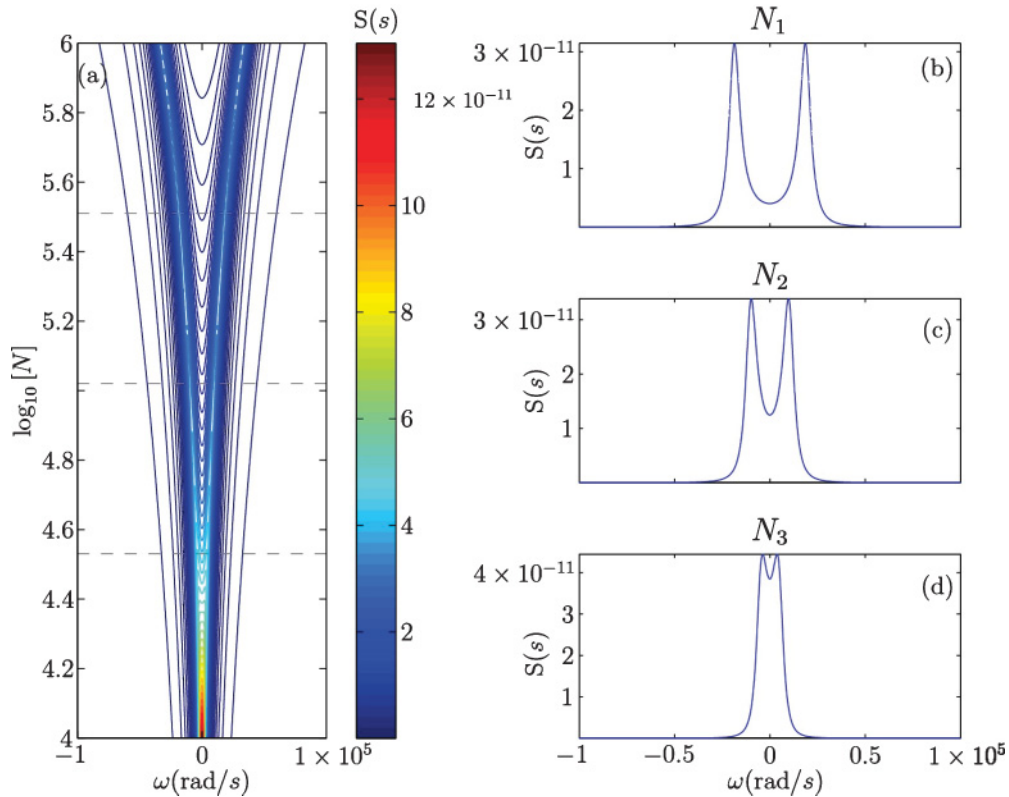


FIG. 8. (Color online) The temperature of the cavity is now set to $T = 0.001$ K ($\bar{n} = 0$) and an incoherent pump of the atoms with $w = 0.05$ is switched on. The spectrum now shows increased emission at the frequencies of the coupled system. Again figures (b)–(d) depict the spectra at $N_1 = 3.2 \times 10^6$, $N_2 = 1 \times 10^6$, and $N_3 = 3.4 \times 10^5$, indicated in (a) by the dashed horizontal lines.

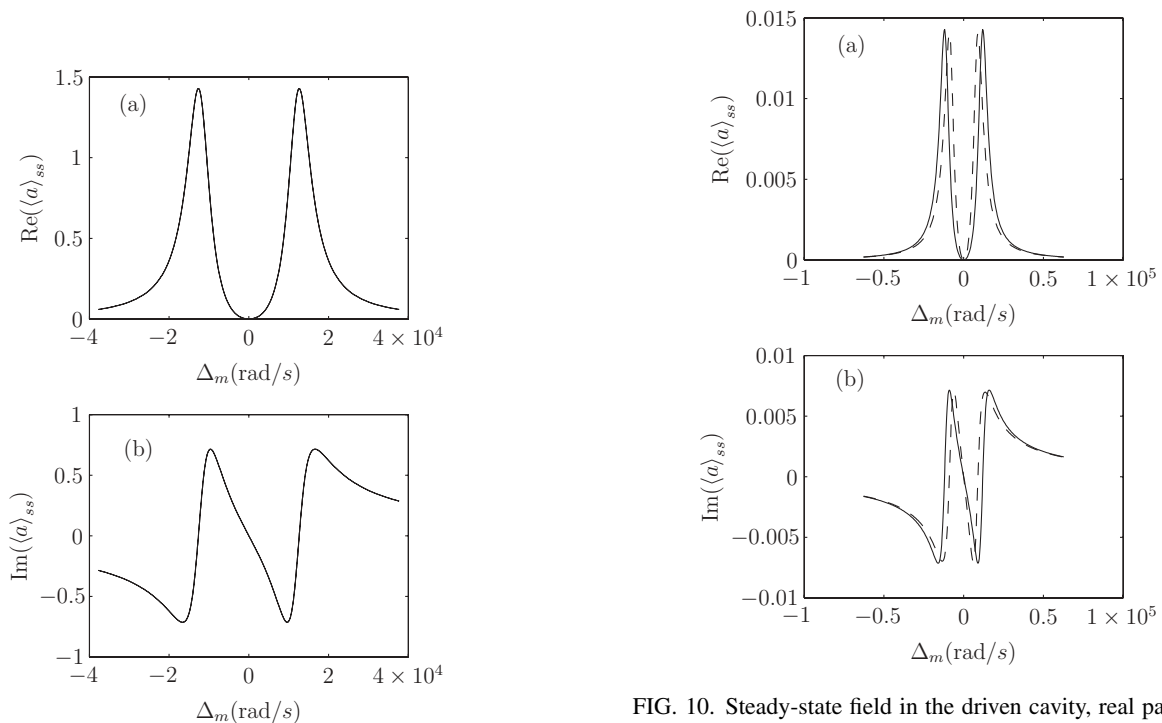


FIG. 9. Steady-state field in the driven cavity, real part (a) and imaginary part (b). The size of the ensemble is chosen to be $N = 10^5$. The lines for $T = 0.01$ K ($\bar{n} = 0$) and $T = 10$ K ($\bar{n} = 30$) coincide.

FIG. 10. Steady-state field in the driven cavity, real part (a) and imaginary part (b), for $T = 0.01$ K ($\bar{n} = 0$) (solid lines) and $T = 10$ K ($\bar{n} = 30$) (dashed lines). For the small ensemble with $N = 10^2$ atoms we recover the effects of the thermal photons. To compensate for the lower number of atoms, the coupling is chosen to $g = 1200$. Otherwise, the splitting would be covered by the cavity linewidth.

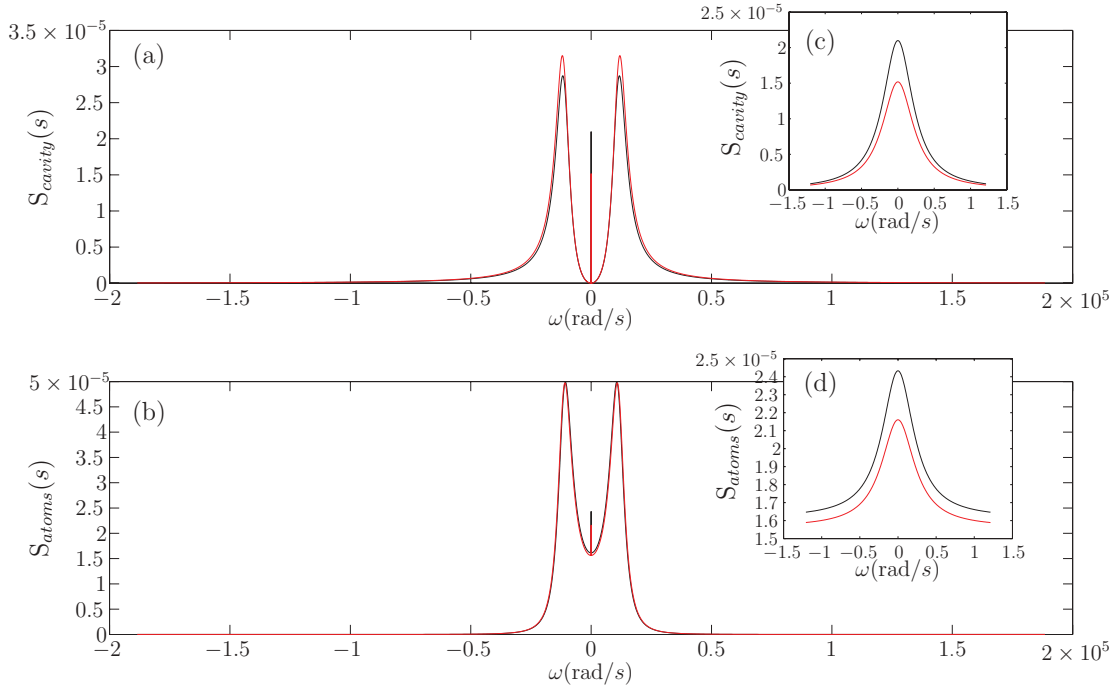


FIG. 11. (Color online) Incoherent spectrum of the mode (a) and of the fluorescence of the ensemble (b) for $T = 0.025$ K, $\kappa = 7 \times 10^3$, $\gamma = 0.3$, $N = 10^5$, $\eta = 9 \times 10^5$ in red (gray), and $\eta = 10^6$ in black. The pump driving the system is on resonance with the cavity and the ensemble. Insets (c) and (d) show a magnification of the central peak of each spectrum. The lower red (gray) line represents the result for $\eta = 9 \times 10^5$.

where we use $\lim_{t \rightarrow \infty} \langle a^\dagger(t)a(t+\tau) \rangle_c \equiv \langle a^\dagger(0)a(\tau) \rangle_c$ and $\lim_{t \rightarrow \infty} \langle \sigma_i^+(t)\sigma_j^-(t+\tau) \rangle_c \equiv \langle \sigma_i^+(0)\sigma_j^-(\tau) \rangle_c$. Equations (24) and (25) couple to four other two-time correlation functions that have to be calculated. To solve for the desired quantities, we Laplace transform both sets of equations and use Cramer's rule to obtain $\langle a^\dagger(0)a(\tau) \rangle_c(s)$ and $\langle \sigma_i^+(0)\sigma_j^-(\tau) \rangle_c(s)$. The necessary steady-state values are obtained numerically.

The incoherent spectra of the mode and of the atoms both show a narrow peak at $\omega_a = \omega_m$ which has a width of $\approx 2\gamma_a$ (see Fig. 11). The double-peaked structure is a remainder of thermal excitations acting as a broad band probe for the ensemble-cavity system. With increasing strength of the coherent pump the narrow central peak becomes dominant. The appearance of the central peak is probably related to weak contributions from almost-dark states (very weakly coupled to the mode). Let us mention in this context that the atomic ensemble is not restricted to a manifold of the Dicke states with fixed J since we include spontaneous emission in our model. It is hence possible that the ensemble ends up in a dark state, where it does not couple to the cavity mode. The time-constant that determines the decay into and the decay of such a dark state is of the order $1/\gamma_a$. This allows for the buildup of long time coherences, and the times the ensemble is in a dark state significantly change the statistics of the photon emission. The result is then a narrow peak in the incoherent spectrum [19,20], where the width of the peak is determined by the characteristic time the ensemble resides in a bright or dark state, in our case γ_a .

In the case of an incoherently pumped ensemble, the narrow peak does not arise. A reason for this can be the nature of the

incoherent pump which is noncollective and hence able to pump the ensemble out of a dark state in a shorter time. This is not possible in the case of the coherently pumped cavity:

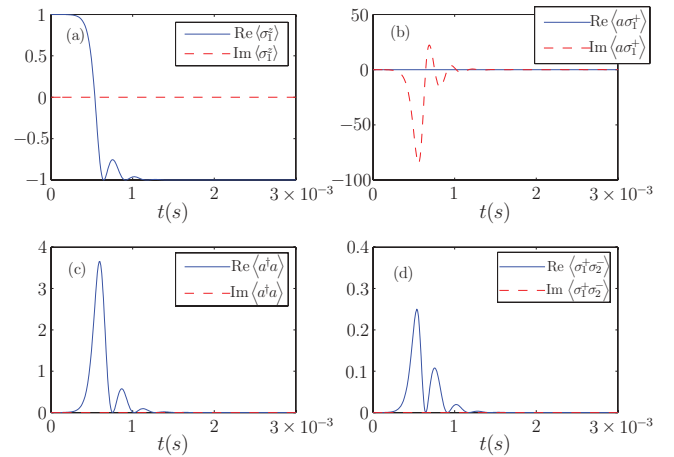


FIG. 12. (Color online) Dynamics of superradiant emission: numerical solutions of the dynamical equations for an ensemble of $N = 10^5$ atoms. The rapid drop of the inversion (σ_1^z) during the emission can be seen in (a). The exchange of excitations between the ensemble and the cavity is characterized by $\langle a\sigma_1^+ \rangle$ in (b). Negative imaginary part of $\langle a\sigma_1^+ \rangle$ indicates emission from the ensemble into the cavity, where a positive imaginary part indicates absorption of cavity photons by the ensemble. In (c) the number of photons in the cavity is depicted. Panel (d) shows the spin-spin correlation $\langle \sigma_1^+ \sigma_2^- \rangle$. In this example the temperature of the mode was chosen to be $T = 4$ K.

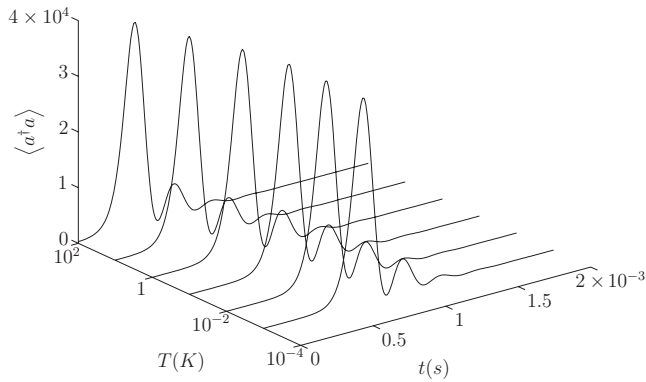


FIG. 13. Dynamics of the photon number in the cavity with increasing temperature. The onset of the superradiant emission is shifted to earlier times since the initially present thermal photons contribute to the fluctuations that trigger the emission process.

Spontaneous emission brings the ensemble to a dark state, but the collective interaction with the mode cannot reach it there.

IV. SUPERRADIANCE

A great advantage of the considered setup is that one has full control of the atomic state. Hence, instead of starting at a

zero-temperature ground state we can prepare an almost fully inverted ensemble, which can feed energy into the system and corresponds to an effective negative temperature [21]. Since we have no initial phase bias in the system, Eqs. (15)–(18) are suitable for describing the dynamics. The resulting superradiant dynamics for an initially fully inverted ensemble is depicted in Fig. 12. In free space the emission occurs in a characteristic burst of duration $\approx \frac{1}{\gamma_a N}$ [22]. The presence of the cavity causes a partial reabsorption of the emitted photons, which can be seen in Fig. 12(c). Due to the large number of emitted photons it should be clearly detectable even on a fairly high thermal background. Following the pulse shape, one also can extract the effective coupling parameters to characterize the system.

The process of superradiance can create a transient entangled state of the ensemble [23]. This entanglement can be revealed by entanglement witnesses which can be inferred from the calculated observables. We have seen some indication of such entanglement appearing. However, the persistence of the entanglement under the influence of noise and with the presence of the cavity will be part of future work.

The onset of superradiant emission is determined by spontaneously emitted photons that trigger the forthcoming burst of radiation. The presence of thermal photons is expected to reduce the time until the onset of the burst. This behavior is recovered by our equations as shown in Fig. 13, where we depict the dynamics of the photon number in the cavity for different temperatures.

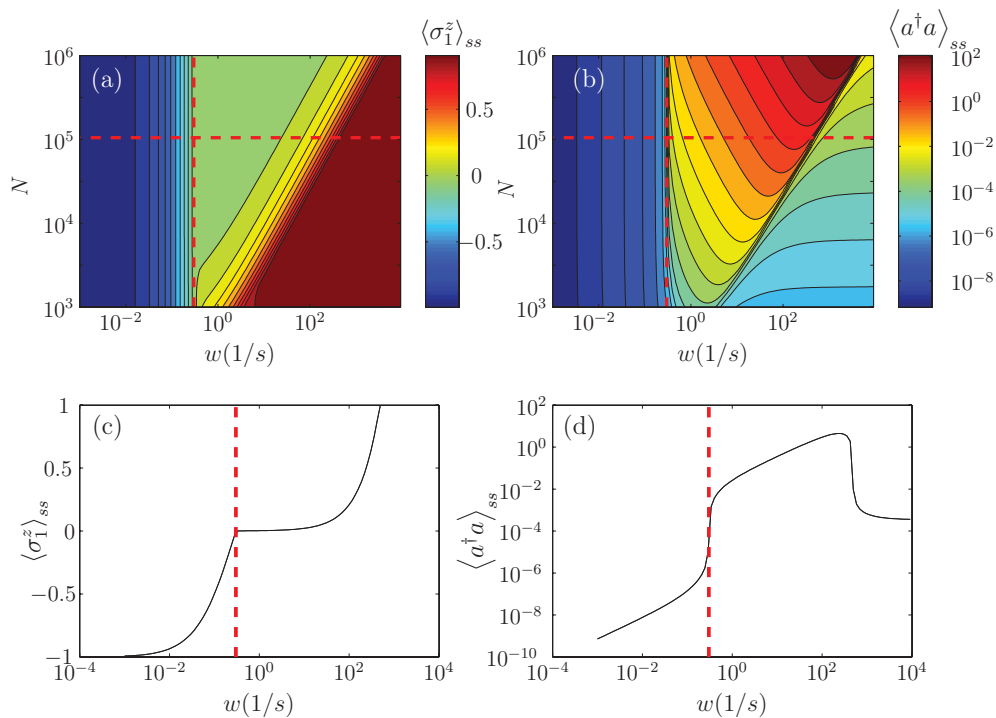


FIG. 14. (Color online) Steady-state inversion of the ensemble (a) and occupation of the cavity mode (b) for varying ensemble size N and pump strength w . The temperature was chosen to be $T_1 = 0.001$ K, which corresponds to an empty cavity ($\bar{n} = 0$). Vertical red dashed lines mark the masing threshold $w = \gamma_a = 0.3$. The horizontal red dashed lines at $N = 10^5$ indicate the position of the curves shown in (c) and (d). From (c) we recover the passage of the inversion through zero for $w = \gamma_a = 0.3$. At this point we see in (d) a rapid increase of the photon number in the mode.

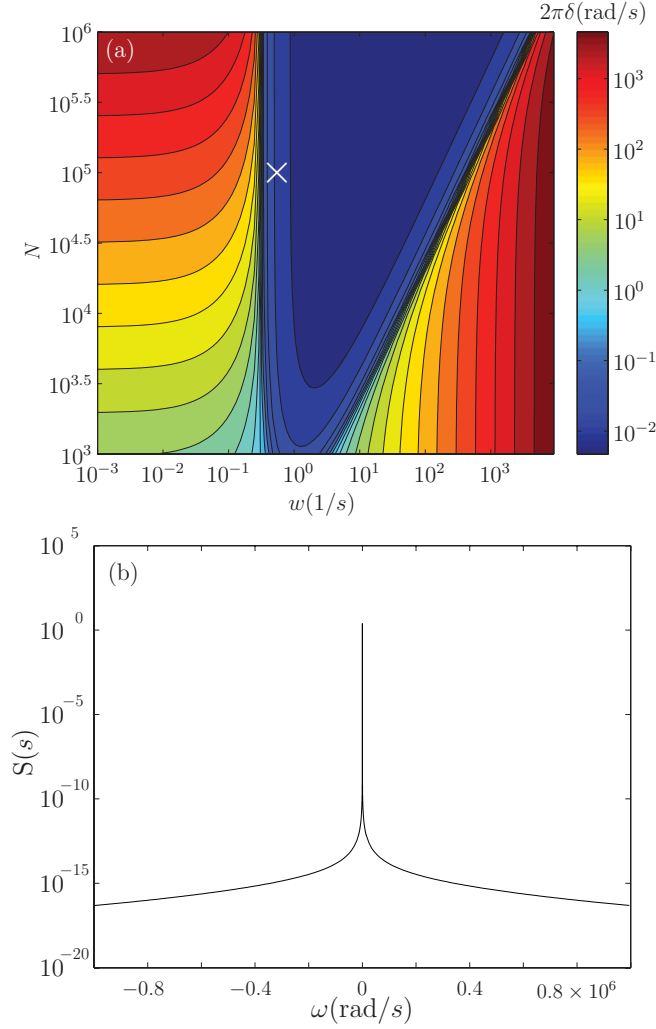


FIG. 15. (Color online) (a) Linewidth of the spectrum $S(\omega)$. For each set of parameters we numerically determine the linewidth of the spectrum. The parameters were chosen to be $\kappa = 7 \times 10^5$, $\gamma_a = 0.3$, $g = 40$, $\omega_m = \omega_a = 2\pi \times 6.83 \times 10^9$, $T = 0.001$. (b) Exemplary spectrum for $N = 10^5$ and $w = 0.55$, marked in (a) by the white cross.

V. NARROWBANDWIDTH HYPERFINE MICROMASER

The collectively coupled ensemble can be used to construct a stripline micromaser with a very low linewidth. To this aim the inversion of the ensemble is sustained by an external incoherent pump of the atoms. In contrast to the calculations in Sec. III C, we ignore the fact that the cavity radiates into a thermally occupied reservoir. After passing the masing threshold, the thermal occupation outside becomes negligible. To determine the linewidth of the emitted light we calculate the Laplace transform of the two-time correlation function $\langle a^\dagger(t)a(0) \rangle$. Using the quantum regression theorem we find

$$\begin{aligned} & \frac{d}{dt} \begin{pmatrix} \langle a^\dagger(t)a(0) \rangle \\ \langle \sigma_1^+(t)a(0) \rangle \end{pmatrix} \\ &= \begin{pmatrix} -\kappa & igN \\ -ig\langle \sigma_1^z \rangle_{ss} & -\frac{w+\gamma_a}{2} \end{pmatrix} \begin{pmatrix} \langle a^\dagger(t)a(0) \rangle \\ \langle \sigma_1^+(t)a(0) \rangle \end{pmatrix}. \end{aligned} \quad (26)$$

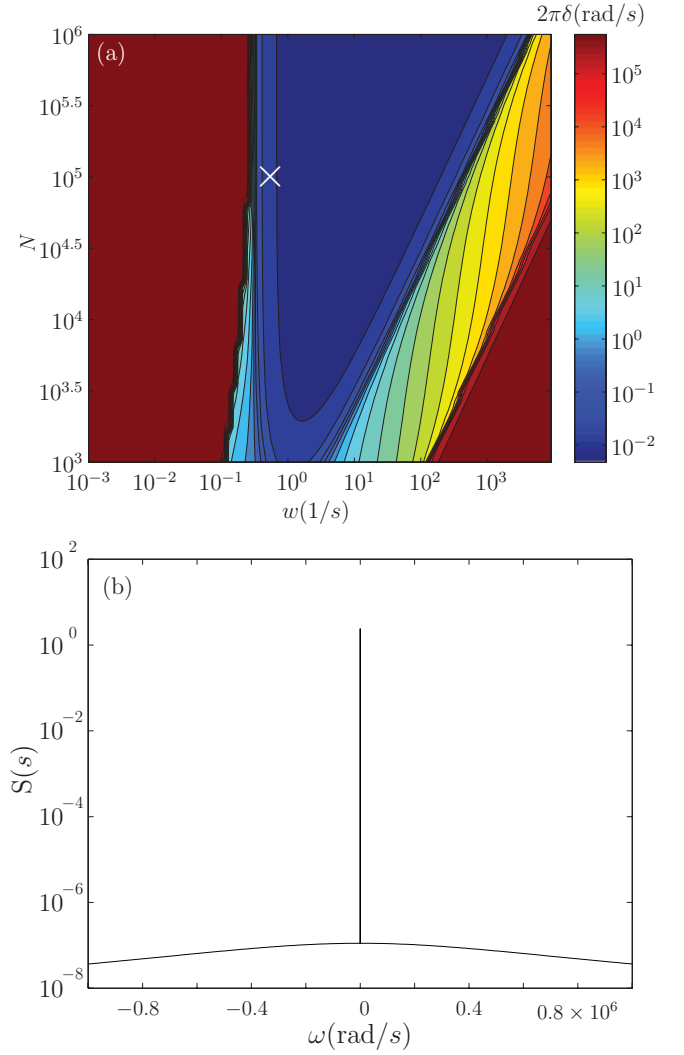


FIG. 16. (Color online) Finite temperature effects in the spectrum. Panel (a) again shows the linewidth of the spectrum. Below the critical pump strength we recover the linewidth of the cavity. The parameters were chosen to be $\kappa = 7 \times 10^5$, $\gamma_a = 0.3$, $g = 40$, $\omega_g = \omega_a = 2\pi \times 6.83 \times 10^9$, $T = 0.1$. (b) Exemplary spectrum for $N = 10^5$ and $w = 0.55$, marked in (a) by the white cross.

Laplace Transform of Eq. (26) gives

$$\begin{pmatrix} \kappa + s & -igN \\ ig\langle \sigma_1^z \rangle_{ss} & \frac{w+\gamma_a}{2} + s \end{pmatrix} \begin{pmatrix} \langle a^\dagger(\tilde{t})a(0) \rangle \\ \langle \sigma_1^+(\tilde{t})a(0) \rangle \end{pmatrix} = \begin{pmatrix} \langle a^\dagger a \rangle_{ss} \\ \langle \sigma_1^+ a \rangle_{ss} \end{pmatrix}, \quad (27)$$

where $\langle \cdot \rangle_{ss}$ denotes steady state values and $\tilde{\cdot}$ denotes Laplace transformed quantities.

The steady-state values on the right-hand side of Eq. (27) can be obtained analytically. Setting the time derivatives of the dynamical equations to zero, a quadratic equation for $\langle \sigma_1^z \rangle_{ss}$ is attained. One of the solutions yields a physically meaningful result for calculating the remaining steady-state values and hence $\langle a^\dagger a \rangle_{ss}$ and $\langle \sigma_1^+ a \rangle_{ss}$. To illustrate the effect of the increasing pump strength, we show the steady-state inversion of the ensemble and the occupation of the cavity in Figs. 14 and 17. Once the critical pump strength is reached, the systems behave identically for different temperatures. The

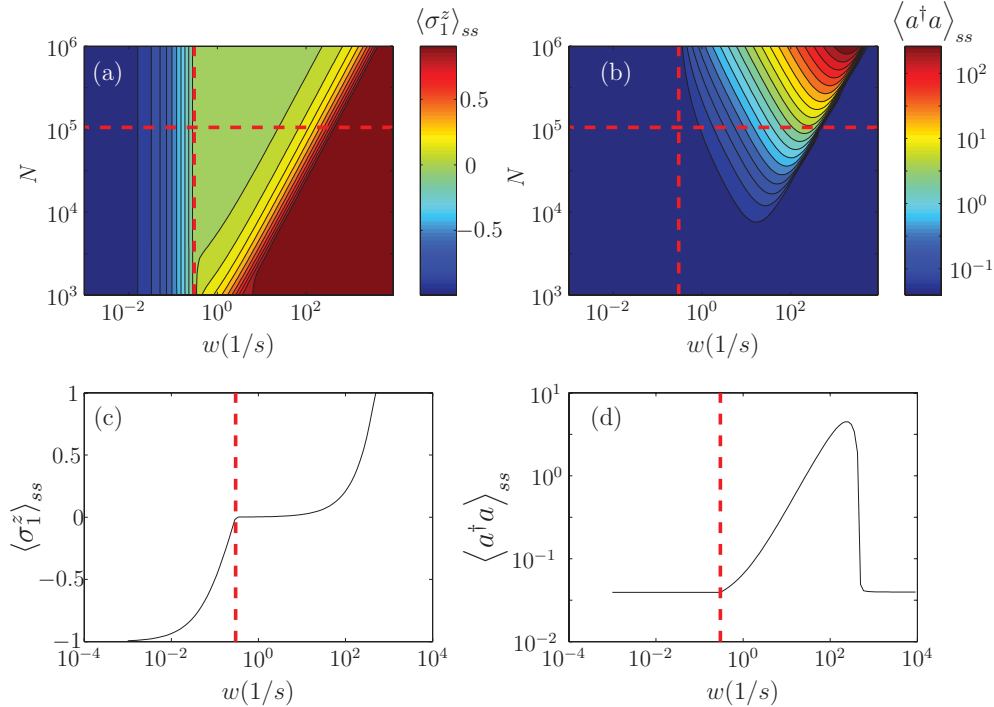


FIG. 17. (Color online) Same as Fig. 14 with $T_2 = 0.1$, which corresponds to $\bar{n} = 0.04$. In (d) the thermal excitations in the mode appear as a constant background from which the increase due to the pump stands out.

number of atoms in the ensemble is varied between 10^3 and 10^6 , whereas the pump parameter w ranges from 10^{-3} to 10^4 . In both figures we mark the pump strength $w = \gamma_a = 0.3$, for which we find the inversion becomes positive, with a vertical red dashed line. At this point we also find a rapid increase of the number of photons in the cavity. The horizontal lines mark the cross sections for $N = 10^5$ shown in what follows.

To solve for $\langle a^\dagger(t)a(0) \rangle$, we use Cramers rule on Eq. (27), which yields

$$\langle a^\dagger(t)\widetilde{a}(0) \rangle(s) = \frac{\langle a^\dagger a \rangle_{ss} \left(\frac{w+\gamma_a}{2} + s \right) - igN \langle \sigma_1^+ a \rangle_{ss}}{(\kappa + s) \left(\frac{w+\gamma_a}{2} + s \right) - g^2 N \langle \sigma_1^z \rangle_{ss}}, \quad (28)$$

so that with $s = -i\omega$ the spectrum is given by

$$S(\omega) = \frac{1}{2\pi} (\langle a^\dagger(t)\widetilde{a}(0) \rangle(\omega) + \langle a^\dagger(t)\widetilde{a}(0) \rangle^*(\omega)). \quad (29)$$

For each set of parameters we calculate the spectrum and determine the linewidth numerically. The linewidth of the maser for two different temperatures $T_1 = 0.001$ K and $T_2 = 0.1$ K is shown in Figs. 15(a) and 16(a). For $w = \gamma_a = 0.3$ we see a rapid drop in the linewidth for both temperatures and a resulting minimal linewidth of $\delta = \frac{1}{2\pi} 4.7 \times 10^{-3}$ Hz. Above the critical pump strength the pump noise destroys the coherence between the individual atoms [9]. In in Figs. 15(b) and 16(b) we plot exemplary spectra for $N = 10^5$ and $w = 0.55$, marked by the white cross.

For $T_2 = 0.1$ K the cavity contains on average $\bar{n} = 0.04$ photons that can be recovered from the constant background in Figs. 17(b) and 17(d). Since the number of thermal photons is small compared to the considered ensembles, the inversion is nonsensitive to the increased temperature.

In Fig. 16 we recover the linewidth of the cavity $\kappa = 7 \times 10^5$ if the pump is below threshold and again if the pump exceeds a critical strength w_{\max} . Above w_{\max} the coherence between different spins is destroyed by the pump noise [9]. The behavior between the threshold and w_{\max} resembles the behavior for $T = 0.001$ K shown in Fig. 15.

VI. CONCLUSIONS

Our studies show that a hybrid cavity QED system consisting of a stripline microwave resonator at finite T and an ensemble of ultracold atoms is a rich and versatile setup for observing and testing prominent quantum physics phenomena. The effectively very cold temperature and good localization of the atomic cloud allow symmetric collective strong coupling to the microwave mode. While the weak magnetic dipole coupling requires large atom numbers and an extremely well localized microwave mode to obtain significant coupling, it also makes the system quite immune to external noise. In addition to the long lifetime of the atomic states, this renders the system an ideal quantum memory or allows for very narrow spectral response or gain. As all the atoms are identical and well trapped, the system exhibits only a very narrow inhomogeneous broadening. Operated in an active way, one thus can envisage a truly microscopic maser with an very narrow linewidth directly locked to an atomic clock transition. The uniform coupling and the possibility of efficient optical pumping enables the study of superradiant decay into the stripline mode, where a precise phase and intensity analysis of the emitted radiation can be performed.

While many of our considerations are guided by parameters expected from an ultracold atom ensemble, it is easy to generalize to alternative setups using NV-centers or other solid-state ensembles. There larger ensembles can be easily envisaged but one also gets much more varying coupling constants and larger inhomogeneous widths. It is not obvious whether the technically more simple setup and larger numbers in this case can compensate for these imperfections.

This could be particularly important for a next step: possible optical readout of the ensemble. For the atomic case, the uniformity of the coupling over many optical wavelengths should allow a nice directional readout of the ensemble state, once a laser could be coupled in.

ACKNOWLEDGMENTS

This work was supported by the Austrian Academy of Sciences and the European Union project MIDAS.

APPENDIX A: COUPLED EQUATIONS

Transformation to a rotating frame with respect to the frequency of the pump ω_l results in $\Delta_m = \omega_m - \omega_l$ for the detuning of the cavity and $\Delta_a = \omega_a - \omega_l$ for the detuning of the atoms. The coupled equations are given by:

$$\frac{d}{dt} \langle a \rangle = -(\kappa + i\Delta_m) \langle a \rangle - igN \langle \sigma_1^- \rangle + \eta, \quad (\text{A1})$$

$$\frac{d}{dt} \langle a^\dagger \rangle = -(\kappa - i\Delta_m) \langle a^\dagger \rangle + igN \langle \sigma_1^+ \rangle + \eta^*, \quad (\text{A2})$$

$$\begin{aligned} \frac{d}{dt} \langle \sigma_1^z \rangle &= -2ig[(\langle \sigma_1^+ a \rangle_c + \langle \sigma_1^+ \rangle \langle a \rangle) - (\langle \sigma_1^- a^\dagger \rangle_c + \langle \sigma_1^- \rangle \langle a^\dagger \rangle)] \\ &\quad - \gamma_a(1 + \langle \sigma_1^z \rangle), \end{aligned} \quad (\text{A3})$$

$$\frac{d}{dt} \langle \sigma_1^- \rangle = -\left(\frac{\gamma_a}{2} + i\Delta_a\right) \langle \sigma_1^- \rangle + ig(\langle \sigma_1^z a \rangle_c + \langle \sigma_1^z \rangle \langle a \rangle), \quad (\text{A4})$$

$$\frac{d}{dt} \langle \sigma_1^+ \rangle = -\left(\frac{\gamma_a}{2} - i\Delta_a\right) \langle \sigma_1^+ \rangle - ig(\langle \sigma_1^z a^\dagger \rangle_c + \langle \sigma_1^z \rangle \langle a^\dagger \rangle), \quad (\text{A5})$$

$$\begin{aligned} \frac{d}{dt} (\langle a\sigma_1^+ \rangle_c + \langle a \rangle \langle \sigma_1^+ \rangle) &= -\left(\kappa + \frac{\gamma_a}{2} + i(\Delta_m - \Delta_a)\right) (\langle a\sigma_1^+ \rangle_c + \langle a \rangle \langle \sigma_1^+ \rangle) \\ &\quad - ig \left(\frac{\langle \sigma_1^z \rangle + 1}{2} + (N-1) \langle \sigma_1^+ \sigma_2^- \rangle_c + \langle \sigma_1^+ \rangle \langle \sigma_2^- \rangle \right) \\ &\quad - ig \langle \sigma_1^z a^\dagger \rangle + \eta \langle \sigma_1^+ \rangle, \end{aligned} \quad (\text{A6})$$

$$\begin{aligned} \frac{d}{dt} (\langle a\sigma_1^z \rangle_c + \langle \sigma_1^z \rangle \langle a \rangle) &= -(\kappa + i\Delta_m) (\langle a\sigma_1^z \rangle_c + \langle \sigma_1^z \rangle \langle a \rangle) + \eta \langle \sigma_1^z \rangle \\ &\quad - 2\gamma_a (\langle a\sigma_1^+ \rangle_c \langle \sigma_1^- \rangle + \langle a\sigma_1^- \rangle_c \langle \sigma_1^+ \rangle + \langle a \rangle \langle \sigma_1^+ \sigma_1^- \rangle) \\ &\quad - ig [2(2\langle \sigma_1^+ a \rangle_c \langle a \rangle + \langle aa \rangle_c \langle \sigma_1^+ \rangle + \langle a \rangle \langle a \rangle \langle \sigma_1^+ \rangle)] \end{aligned}$$

$$\begin{aligned} &- (1 + 2\langle a^\dagger a \rangle_c) \langle \sigma_1^- \rangle - 2\langle a\sigma_1^- \rangle_c \langle a^\dagger \rangle \\ &- 2\langle a^\dagger \sigma_1^- \rangle_c \langle a \rangle - 2\langle a^\dagger \rangle \langle a \rangle \langle \sigma_1^- \rangle \\ &+ (N-1) (\langle \sigma_1^z \sigma_2^- \rangle_c + \langle \sigma_1^z \rangle \langle \sigma_2^- \rangle), \end{aligned} \quad (\text{A7})$$

$$\begin{aligned} \frac{d}{dt} (\langle \sigma_1^+ \sigma_2^- \rangle_c + \langle \sigma_1^+ \rangle \langle \sigma_2^- \rangle) &= -ig [\langle \sigma_1^z \sigma_2^- \rangle_c \langle a^\dagger \rangle + \langle \sigma_1^z a^\dagger \rangle_c \langle \sigma_1^- \rangle + \langle \sigma_1^- a^\dagger \rangle_c \langle \sigma_1^z \rangle \\ &\quad + \langle \sigma_1^- \rangle \langle \sigma_1^z \rangle \langle a^\dagger \rangle - (\langle \sigma_1^z \sigma_2^+ \rangle_c \langle a \rangle + \langle \sigma_1^z a \rangle_c \langle \sigma_1^+ \rangle \\ &\quad + \langle \sigma_1^+ a \rangle_c \langle \sigma_1^z \rangle + \langle \sigma_1^+ \rangle \langle \sigma_1^z \rangle \langle a \rangle)] \\ &\quad - \gamma_a (\langle \sigma_1^+ \sigma_2^- \rangle_c + \langle \sigma_1^+ \rangle \langle \sigma_2^- \rangle), \end{aligned} \quad (\text{A8})$$

$$\begin{aligned} \frac{d}{dt} (\langle a^\dagger a \rangle_c + \langle a^\dagger \rangle \langle a \rangle) &= -igN [(\langle a^\dagger \sigma_1^- \rangle_c + \langle a^\dagger \rangle \langle \sigma_1^- \rangle) - (\langle a\sigma_1^+ \rangle_c + \langle a \rangle \langle \sigma_1^+ \rangle)] \\ &\quad - 2\kappa (\langle a^\dagger a \rangle_c + \langle a^\dagger \rangle \langle a \rangle) + 2\kappa \bar{n} + \eta^* \langle a \rangle + \eta \langle a^\dagger \rangle, \end{aligned} \quad (\text{A9})$$

$$\begin{aligned} \frac{d}{dt} (\langle a\sigma_1^- \rangle_c + \langle a \rangle \langle \sigma_1^- \rangle) &= -\left(i(\Delta_m + \Delta_a) + \kappa + \frac{\gamma_a}{2}\right) (\langle a\sigma_1^- \rangle_c + \langle a \rangle \langle \sigma_1^- \rangle) \\ &\quad - ig(N-1) (\langle \sigma_1^- \sigma_2^- \rangle_c + \langle \sigma_1^- \rangle \langle \sigma_2^- \rangle) + \eta \langle \sigma_1^- \rangle \\ &\quad + ig(2\langle \sigma_1^z a \rangle_c \langle a \rangle + \langle aa \rangle_c \langle \sigma_1^z \rangle + \langle a \rangle \langle a \rangle \langle \sigma_1^z \rangle), \end{aligned} \quad (\text{A10})$$

$$\begin{aligned} \frac{d}{dt} (\langle a^\dagger a^\dagger \rangle_c - \langle a^\dagger \rangle \langle a^\dagger \rangle) &= -(2\kappa - i2\Delta_m) (\langle a^\dagger a^\dagger \rangle_c - \langle a^\dagger \rangle \langle a^\dagger \rangle) \\ &\quad + 2igN (\langle \sigma_1^+ a^\dagger \rangle_c + \langle a^\dagger \rangle \langle \sigma_1^+ \rangle) + 2\eta^* \langle a^\dagger \rangle, \end{aligned} \quad (\text{A11})$$

$$\begin{aligned} \frac{d}{dt} (\langle \sigma_1^- \sigma_2^- \rangle_c + \langle \sigma_1^- \rangle \langle \sigma_2^- \rangle) &= -2\left(\frac{\gamma_a}{2} + i\Delta_a\right) (\langle \sigma_1^- \sigma_2^- \rangle_c + \langle \sigma_1^- \rangle \langle \sigma_2^- \rangle) + i2g (\langle \sigma_1^z \sigma_2^- \rangle_c \langle a \rangle \\ &\quad + \langle \sigma_1^z a \rangle_c \langle \sigma_1^- \rangle + \langle \sigma_1^- a \rangle_c \langle \sigma_1^z \rangle + \langle \sigma_1^z \rangle \langle \sigma_1^- \rangle \langle a \rangle), \end{aligned} \quad (\text{A12})$$

$$\begin{aligned} \frac{d}{dt} (\langle \sigma_1^z \sigma_2^+ \rangle_c + \langle \sigma_1^z \rangle \langle \sigma_2^+ \rangle) &= \left(-\frac{\gamma_a}{2} + i\Delta_a\right) (\langle \sigma_1^z \sigma_2^+ \rangle_c + \langle \sigma_1^z \rangle \langle \sigma_2^+ \rangle) \\ &\quad - 2\gamma_a (\langle \sigma_1^+ \sigma_1^- \rangle_c \langle \sigma_1^+ \rangle + \langle \sigma_1^+ \sigma_2^+ \rangle_c \langle \sigma_1^- \rangle + \langle \sigma_1^- \sigma_2^+ \rangle_c \langle \sigma_1^+ \rangle) \\ &\quad - ig [2(\langle \sigma_1^+ \sigma_2^+ \rangle_c \langle a \rangle + 2\langle \sigma_1^+ a \rangle_c \langle \sigma_1^+ \rangle \\ &\quad + \langle \sigma_1^+ \rangle \langle \sigma_1^+ \rangle \langle a \rangle - \langle \sigma_1^- \sigma_2^+ \rangle_c \langle a^\dagger \rangle \\ &\quad - \langle \sigma_1^- a^\dagger \rangle_c \langle \sigma_1^+ \rangle - \langle \sigma_1^+ a^\dagger \rangle_c \langle \sigma_1^- \rangle - \langle \sigma_1^+ \rangle \langle \sigma_1^- \rangle \langle a^\dagger \rangle) \\ &\quad + \langle \sigma_1^z \sigma_2^- \rangle_c \langle a^\dagger \rangle + 2\langle \sigma_1^z a^\dagger \rangle_c \langle \sigma_1^z \rangle + \langle \sigma_1^z \rangle \langle \sigma_1^z \rangle \langle a^\dagger \rangle], \end{aligned} \quad (\text{A13})$$

$$\begin{aligned} \frac{d}{dt} (\langle \sigma_1^z \sigma_2^z \rangle_c + \langle \sigma_1^z \rangle \langle \sigma_2^z \rangle) &= -4ig (\langle \sigma_1^z \sigma_2^+ \rangle_c \langle a \rangle + \langle \sigma_1^z a \rangle_c \langle \sigma_1^+ \rangle + \langle \sigma_1^+ a \rangle_c \langle \sigma_1^z \rangle \\ &\quad + \langle a \rangle \langle \sigma_1^z \rangle \langle \sigma_1^+ \rangle - \langle \sigma_1^- \sigma_2^z \rangle_c \langle a^\dagger \rangle - \langle \sigma_1^z a^\dagger \rangle_c \langle \sigma_1^- \rangle \\ &\quad - \langle \sigma_1^- a^\dagger \rangle_c \langle \sigma_1^z \rangle - \langle a^\dagger \rangle \langle \sigma_1^- \rangle \langle \sigma_1^z \rangle) - 4\gamma_a (\langle \sigma_1^+ \sigma_1^- \rangle_c \langle \sigma_1^z \rangle \\ &\quad + \langle \sigma_1^+ \sigma_2^z \rangle_c \langle \sigma_1^- \rangle + \langle \sigma_1^- \sigma_2^z \rangle_c \langle \sigma_1^+ \rangle). \end{aligned} \quad (\text{A14})$$

APPENDIX B: VALIDITY OF THE CUMULANT EXPANSION

The validity of the truncation of the expansion performed previously relies on the assumption that higher-order cumulants are negligible. This can be checked in principle by truncating at higher orders and comparing the results. In general, it turns out that there is one cumulant which requires more care: the correlation between the inversion and the photon number $\langle a^\dagger a \sigma_1^z \rangle$. In the regime where $\frac{g_{\text{eff}}}{\kappa} > 1$ and $\frac{g_{\text{eff}}}{\gamma_a} > 1$ holds, the number of photons necessary to saturate the ensemble is low. Therefore small fluctuations of the photon number can cause significant changes in the inversion [24]. The correlation between the photon number and the inversion $\langle a^\dagger a \sigma_1^z \rangle_c$ is therefore kept in our calculations. Hence, an expansion like in Eq. (14) would not be advantageous because none of the terms could be dropped. We therefore calculate the dynamical equation for $\langle a^\dagger a \sigma_1^z \rangle$ which gives

$$\begin{aligned} \frac{d}{dt} \langle a^\dagger a \sigma_1^z \rangle &= (-2\kappa - \gamma_a) \langle a^\dagger a \sigma_1^z \rangle - \gamma_a \langle a^\dagger a \rangle + 2\kappa \bar{n} \langle \sigma_1^z \rangle \\ &\quad - ig[\langle a \sigma_1^+ \rangle - \langle a^\dagger \sigma_1^- \rangle + 2(\langle a^\dagger a a \sigma_1^+ \rangle - \langle a^\dagger a^\dagger a \sigma_1^- \rangle)] \\ &\quad - ig(N-1)(\langle a^\dagger \sigma_1^z \sigma_2^- \rangle - \langle a \sigma_1^z \sigma_2^+ \rangle) \\ &\quad + \eta \langle a^\dagger \sigma_1^z \rangle + \eta^* \langle a \sigma_1^z \rangle. \end{aligned} \quad (\text{B1})$$

The expectation values of products of three operators are expanded as in Eq. (14), except for $\langle a^\dagger a \sigma_1^z \rangle$. The expansion of expectation values with four operators is more involved and produces also expectation values of products of three operators which are again expanded. Cumulants of order three and four are neglected. The resulting equation for $\langle a^\dagger a \sigma_1^z \rangle$ can be integrated numerically along with the equations for the other quantities mentioned previously.

To estimate the influence of the correlation between the photon number and the inversion $\langle a^\dagger a \sigma_1^z \rangle_c$ on the dynamics, we plot the photon number in the cavity during the decay of a fully inverted ensemble. We therefore integrate a set of 12 equations that is obtained if $\langle a^\dagger a \sigma_1^z \rangle$ is expanded and $\langle a^\dagger a \sigma_1^z \rangle_c$ is neglected. For comparison, we also show the dynamics obtained from the full set of 13 equations in which $\langle a^\dagger a \sigma_1^z \rangle_c$ is kept [see Fig. 18(a)].

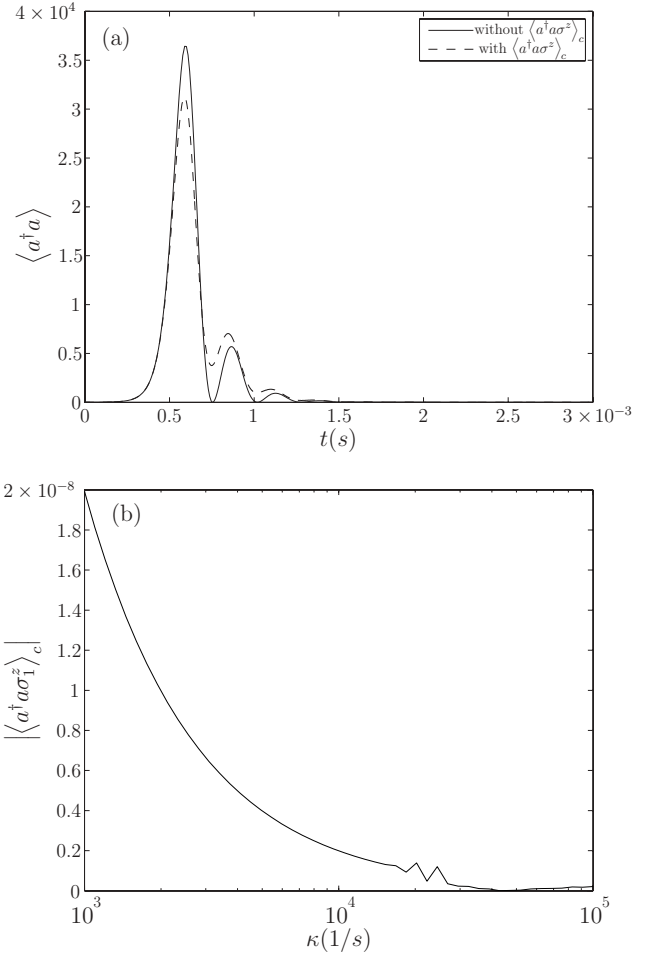


FIG. 18. (a) Dynamics of the photon number in the cavity mode for an initially fully inverted ensemble. The solid line shows the dynamics produced by the set of equations where $\langle a^\dagger a \sigma_1^z \rangle_c$ was neglected. The dashed curve is the result of the full set of 13 equations in which $\langle a^\dagger a \sigma_1^z \rangle_c$ is kept. (b) Numerically obtained cumulant $\langle a^\dagger a \sigma_1^z \rangle_c$ in the steady state. With increasing loss rate of the cavity κ the correlation between photon number and inversion decreases.

The steady state of both solutions differs only slightly. The correlation $\langle a^\dagger a \sigma_1^z \rangle_c$ is shown in Fig. 18(b). With increasing cavity decay rate κ the correlation between photon number and inversion decreases.

[1] M. Tavis and F. Cummings, *Phys. Rev.* **170**, 379 (1968).
 [2] L. Duan, M. Lukin, J. Cirac, and P. Zoller, *Nature (London)* **414**, 413 (2001).
 [3] P. Rabl, D. DeMille, J. Doyle, M. Lukin, R. Schoelkopf, and P. Zoller, *Phys. Rev. Lett.* **97**, 033003 (2006).
 [4] A. Imamoglu, *Phys. Rev. Lett.* **102**, 083602 (2009).
 [5] J. Verdu, H. Zoubi, C. Koller, J. Majer, H. Ritsch, and J. Schmiedmayer, *Phys. Rev. Lett.* **103**, 043603 (2009).
 [6] A. Wallraff, D. Schuster, A. Blais, L. Frunzio, R. Huang, J. Majer, S. Kumar, S. Girvin, and R. Schoelkopf, *Nature (London)* **431**, 162 (2004).

[7] P. Böhi, M. Riedel, J. Hoffrogge, J. Reichel, T. Hänsch, and P. Treutlein, *Nat. Phys.* **5**, 592 (2009).
 [8] M. R. Matthews, D. S. Hall, D. S. Jin, J. R. Ensher, C. E. Wieman, E. A. Cornell, F. Dalfovo, C. Minniti, and S. Stringari, *Phys. Rev. Lett.* **81**, 243 (1998).
 [9] D. Meiser, J. Ye, D. R. Carlson, and M. J. Holland, *Phys. Rev. Lett.* **102**, 163601 (2009).
 [10] S. Haroche and J. Raimond, *Exploring the Quantum: Atoms, Cavities and Photons* (Oxford University Press, New York, 2006).
 [11] R. Dicke, *Phys. Rev.* **93**, 99 (1954).

- [12] F. Haake, M. Kolobov, C. Fabre, E. Giacobino, and S. Reynaud, *Phys. Rev. Lett.* **71**, 995 (1993).
- [13] B. Kasch, H. Hattermann, D. Cano, T. E. Judd, S. Scheel, C. Zimmermann, R. Kleiner, D. Koelle, and J. Fortágh, *New J. Phys.* **12**, 065024 (2010).
- [14] C. Gardiner, *Handbook of Stochastic Methods* (Springer, Berlin, 1985).
- [15] H. Carmichael, *Statistical Methods in Quantum Optics* (Springer, Berlin, 1999).
- [16] S. Tan, *J. Opt. B* **1**, 424 (1999).
- [17] R. Kubo, *J. Phys. Soc. Jpn.* **17**, 1100 (1962).
- [18] H. Carmichael, *J. Opt. Soc. Am. B* **4**, 1588 (1987).
- [19] M. Plenio and P. Knight, *Rev. Mod. Phys.* **70**, 101 (1998).
- [20] P. Zoller, M. Marte, and D. F. Walls, *Phys. Rev. A* **35**, 198 (1987).
- [21] C. Gardiner and P. Zoller, *Quantum Noise* (Springer, Berlin, 1991).
- [22] M. Gross and S. Haroche, *Phys. Rep.* **93**, 301 (1982).
- [23] P. Milman, *Phys. Rev. A* **74**, 042317 (2006).
- [24] P. R. Rice and H. J. Carmichael, *Phys. Rev. A* **50**, 4318 (1994).